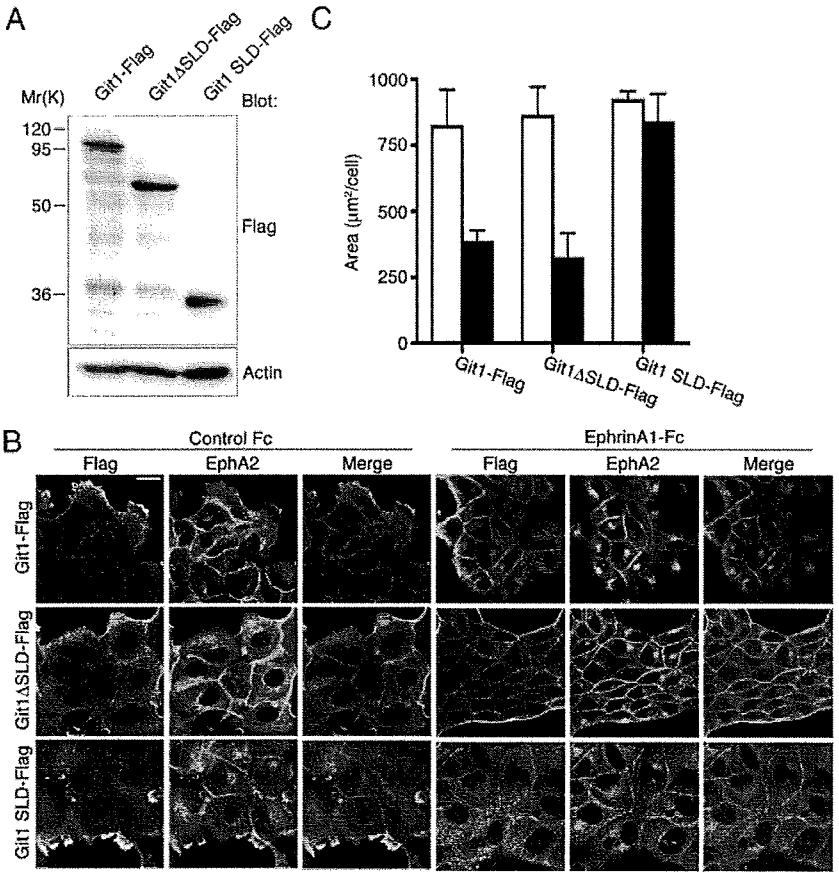

Figure 7. Subcellular localization of EphA2 and Git1 in MDCK cells. (A) Expression of Git1-FLAG or its mutants, as detected by anti-FLAG immunoblots of total cell lysates (10 μg). Anti-actin immunoblots are shown as a control. (B and C) Colocalization of Git1, and its mutants, with EphA2 in ephrinA1-Fc-treated MDCK cells (B), and their effects on cell compaction (C). Cells stably expressing Git1-FLAG or its mutants were cultured under the sparse density and treated with ephrinA1-Fc or control Fc for 1 h, before being labeled with an anti-FLAG antibody coupled with an Alexa 488-labeled anti-mouse IgG antibody (green) and an anti-EphA2 antibody coupled with an Alexa 555-labeled anti-rabbit IgG antibody (magenta). Bar, 20 μm (B). In C, open bars, control Fc; closed bars, ephrinA1-Fc.

upon ephrinA1-Fc stimulation and colocalizes well with EphA2 (Figure 7B). The synaptic localizing domain of Git1 was previously identified as being responsible for its localization to neuronal synapses (Zhang *et al.*, 2003). In MDCK cells, however, we found that Git1ΔSLD-FLAG, which lacks the synaptic localizing domain, is still able to localize to cell–cell contacts, although with a lower efficiency than that of intact Git1-FLAG (Figure 7, B and C). In contrast, expression of the synaptic localizing domain alone (Git1 SLD-FLAG) blocked ephrinA1–Fc-mediated cell compaction, whereas this domain alone seemed to be very inefficient in localizing to the cell–cell contacts (Figure 7, B and C). These results again suggest the importance of the synaptic localizing domain of Git1 in Eph signaling, although this domain per se is not essential for its localization to cell–cell contacts.

DISCUSSION

EphA receptors have been implicated in the inhibition of cell migration and growth. To accomplish such roles, several EphA receptors have been shown to employ signaling molecules that down-regulate the activities of Ras and Rac small GTPases, such as p120RasGAP and α-chimaerin (Pasquale, 2005, 2008). In this paper, we show that EphA2 has a novel signaling pathway that downregulates the activity of another small GTPase, Arf6, by recruiting Git1. Through this pathway, we show that the ligand-activation of EphA2, which may occur during cell-cell contacting of epithelial cells, contributes to the cell compaction as well as the maturation of E-cadherin-based cell-cell adhesion and apical-basal polarization. Our results also show that E-cadherin function is necessary for the EphA2-mediated down-regulation of the Arf6 activity during cell-cell contacting. Therefore, it is plausible to assume that a positive feedback loop exists between EphA2 and E-cadherin in some normal epithelial cells, in which E-cadherin-based cell-cell contacts enhance binding of EphA2 receptors with their ligands, which in turn activates the signaling pathway at the cell-cell contacting areas to down-regulate Arf6 activity, and this down-regulation then acts to enhance E-cadherin-based cell-cell adhesions as well as maturation of apical-basal polarization.

Git1 has been shown to localize and function at cell–cell junctions formed in neuronal synapses (Zhang *et al.*, 2003) and immune synapses (Phee *et al.*, 2005). However, these studies have mostly dealt with Git1 as a scaffold protein, which links cell surface receptors to the Pix–Pak pathway to remodel actin cytoskeletal architecture and stabilize these cell–cell junctions. In contrast, our present study clarifies the role of Git1 as a GTPase-activating protein for Arf6 in the stabilization of cell–cell junctions.

We show that EphA2 signaling causes enhanced polarization in the apical-to-basal direction, which is accompanied by clear segregation of ZO-1 and Ezrin from E-cadherin. Interestingly, suppression of Git1 and Nck1 expression also affects the subcellular localization of ZO-1. Therefore, activation of the EphA2–Nck1–Git1 signaling pathway seems to lead to maturation of tight junction structures, together with the maturation of adherens junctions. In contrast, it has been shown that an active form of the Arf6 mutant does not

perturb localization of ZO-1 at cell–cell contacts in MDCK cells under a condition in which this mutant disrupts E-cadherin–based adherens junctions (Palacios *et al.*, 2001). It will be interesting to investigate whether the EphA2–Nck1–Git1 pathway, as well as the GAP activity of Git1, is directly involved also in the maturation of tight junctions. Moreover, Eph receptor signaling also regulates activities of other small GTPases, including Rac1, RhoA, and Rap1 (Pasquale, 2005), which may also be involved in modulating the architecture of cell–cell adhesions. In particular, it has been shown that Rac1 activities can be tightly coupled with activities of Arf6 (Radhakrishna *et al.*, 1999). It will be interesting to examine whether EphA2 signaling, as well as cell densities affect activities of other small GTPases.

Penela *et al.* (2008) have reported that Git1 plays a role in enhancing cell migration and proliferation of HeLa cells and COS7 cells, by interacting with G protein-coupled receptor kinase 2. These cells are completely transformed; moreover, HeLa cells have lost the expression of E-cadherin. Their report, together with our results suggest that Git1 may be pleiotropic, having different roles in different signaling pathways or cellular contexts. It will be interesting to examine whether Git1 also acts as a GAP for Arf6 in G protein-coupled receptor signaling or just acts as a scaffold protein in this signaling pathway.

The synaptic localizing domain of Git1 contains both typical and atypical PXXP motifs at its C terminus and has been predicted to bind to some yet unidentified SH3 domains (Bagrodia *et al.*, 1999). We show that the Nck1 SH3 domain binds to this synaptic localizing domain, an interaction which requires the C-terminal proline-rich region of this synaptic localizing domain. Recently, it was reported that Git1 forms a closed conformation by intramolecular interaction between its N- and C-terminal regions. When the synaptic localizing domain or the Ankyrin repeat is deleted, Git1 seems to change to an open conformation and shows increased affinities to paxillin and liprin α (Totaro *et al.*, 2007). We observed that the synaptic localizing domain of Git1 alone shows higher affinity to the Nck SH3 domain than full-length Git1 (data not shown). Therefore, it will be interesting to examine whether Eph signals have a role in changing Git1 to an open conformation and hence up-regulating its binding to other proteins. It will also be interesting to examine whether Eph signals up-regulate the GAP activity of Git1.

Disruption of E-cadherin–mediated cell–cell adhesions is the major cause for the acquisition of invasive and metastatic properties in most types of carcinomas (Takeichi, 1991). The *EphA2* gene has been implicated in tumor suppression, as mentioned. It will thus be interesting to clarify the precise molecular mechanism by which Arf6 activity, which is under the regulation of the EphA2–Nck–Git1 signaling pathway, participates in the processes maintaining E-cadherin–mediated cell–cell adhesions, especially those regulating the cellular dynamics and fates of E-cadherin molecules. Moreover, loss of EphB receptors have also been highly implicated in the tumorigenesis of different types of cancers (Pasquale, 2008), and EphB signaling has also been shown to enhance cell–cell adhesion by recruiting E-cadherin to the plasma membrane (Cortina *et al.*, 2007). Furthermore, EphB receptors possess Nck SH2 binding sites (Kullander and Klein, 2002). It will thus be interesting to examine whether EphB receptors also use a similar pathway involving the suppression of Arf6 activity.

ACKNOWLEDGMENTS

We are grateful to T. Yoneda, Y. Shibata, A. Arakawa, M. Minamimoto, and M. Hiraishi for technical assistance and Y. Okuda for secretarial work. We also thank M. Takeichi, A. Miyawaki, K. Nakayama, and T. Shishido for cDNAs; Sh. Tsukita for cells; Y. Mazaki and A. Suzuki for technical suggestions; and H. A. Popiel for critical reading of the manuscript. This work was supported in part by grants-in-aid from the Ministry of Education, Science, Sports and Culture of Japan and by the Takeda Science Foundation.

REFERENCES

Bagrodia, S., Bailey, D., Lenard, Z., Hart, M., Guan, J. L., Premont, R. T., Taylor, S. J., and Cerione, R. A. (1999). A tyrosine-phosphorylated protein that binds to an important regulatory region on the cool family of p21-activated kinase-binding proteins. J. Biol. Chem. *274*, 22393–22400.

Bauer, T., Motosugi, N., Miura, K., Sabe, H., and Hiiragi, T. (2008). Dynamic rearrangement of surface proteins is essential for cytokinesis. Genesis *46*, 152–162.

Becker, E., Huynh-Do, U., Holland, S., Pawson, T., Daniel, T. O., and Skolnik, E. Y. (2000). Nck-interacting Ste20 kinase couples Eph receptors to c-Jun N-terminal kinase and integrin activation. Mol. Cell. Biol. *20*, 1537–1545.

Cortina, C., *et al.* (2007). EphB-ephrin-B interactions suppress colorectal cancer progression by compartmentalizing tumor cells. Nat. Genet. *39*, 1376–1383.

Donaldson, J. G. (2003). Multiple roles for Arf *6*, sorting, structuring, and signaling at the plasma membrane. J. Biol. Chem. *278*, 41573–41576.

Frese, S., Schubert, W. D., Findeis, A. C., Marquardt, T., Roske, Y. S., Stradal, T. E., and Heinz, D. W. (2006). The phosphotyrosine peptide binding specificity of Nck1 and Nck2 Src homology 2 domains. J. Biol. Chem. *281*, 18236–18245.

Gumbiner, B. M. (2005). Regulation of cadherin-mediated adhesion in morphogenesis. Nat. Rev. Mol. Cell Biol. *6*, 622–634.

Guo, H., Miao, H., Gerber, L., Singh, J., Denning, M. F., Gilliam, A. C., and Wang, B. (2006). Disruption of EphA2 receptor tyrosine kinase leads to increased susceptibility to carcinogenesis in mouse skin. Cancer Res. *66*, 7050–7058.

Hiroi, T., Someya, A., Thompson, W., Moss, J., and Vaughan, M. (2006). GEP100/BRAG 2, activator of ADP-ribosylation factor 6 for regulation of cell adhesion and actin cytoskeleton via E-cadherin and α-catenin. Proc. Natl. Acad. Sci. USA *103*, 10672–10677.

Hoefen, R. J., and Berk, B. C. (2006). The multifunctional GIT family of proteins. J. Cell Sci. *119*, 1469–1475.

Kullander, K., and Klein, R. (2002). Mechanisms and functions of Eph and ephrin signalling. Nat. Rev. Mol. Cell Biol. *3*, 475–486.

Laprise, P., Langlois, M. J., Boucher, M. J., Jobin, C., and Rivard, N. (2004). Down-regulation of MEK/ERK signaling by E-cadherin-dependent PI3K/Akt pathway in differentiating intestinal epithelial cells. J. Cell. Physiol. *199*, 32–39.

Macrae, M., Neve, R. M., Rodriguez-Viciana, P., Haqq, C., Yeh, J., Chen, C., Gray, J. W., and McCormick, F. (2005). A conditional feedback loop regulates Ras activity through EphA2. Cancer Cell *8*, 111–118.

Mazaki, Y., *et al.* (2001). An ADP-ribosylation factor GTPase-activating protein Git2-short/KIAA0148 is involved in subcellular localization of paxillin and actin cytoskeletal organization. Mol. Biol. Cell *12*, 645–662.

Meyer, M. Z., Deliot, N., Chasserot-Golaz, S., Premont, R. T., Bader, M. F., and Vitale, N. (2006). Regulation of neuroendocrine exocytosis by the ARF6 GTPase-activating protein GIT1. J. Biol. Chem. *281*, 7919–7926.

Miao, H., Burnett, E., Kinch, M., Simon, E., and Wang, B. (2000). Activation of EphA2 kinase suppresses integrin function and causes focal-adhesion-kinase dephosphorylation. Nat. Cell Biol. *2*, 62–69.

Miao, H., Nickel, C. H., Cantley, L. G., Bruggeman, L. A., Bennardo, L. N., and Wang, B. (2003). EphA kinase activation regulates HGF-induced epithelial branching morphogenesis. J. Cell Biol. *162*, 1281–1292.

Miao, H., Wei, B. R., Peehl, D. M., Li, Q., Alexandrou, T., Schelling, J. R., Rhim, J. S., Sedor, J. R., Burnett, E., and Wang, B. (2001). Activation of EphA receptor tyrosine kinase inhibits the Ras/MAPK pathway. Nat. Cell Biol. *3*, 527–530.

Morishige, M., *et al.* (2008). GEP100 links epidermal growth factor receptor signalling to Arf6 activation to induce breast cancer invasion. Nat. Cell Biol. *10*, 85–92.

Noblitt, L. W., Bangari, D. S., Shukla, S., Knapp, D. W., Mohammed, S., Kinch, M. S., and Mittal, S. K. (2004). Decreased tumorigenic potential of EphA2-overexpressing breast cancer cells following treatment with adenoviral vectors that express EphrinA1. Cancer Gene Ther. *11*, 757–766.

Noren, N. K., Foos, G., Hauser, C. A., and Pasquale, E. B. (2006). The EphB4 receptor suppresses breast cancer cell tumorigenicity through an Abl-Crk pathway. Nat. Cell Biol. *8*, 815–825.

Palacios, F., Price, L., Schweitzer, J., Collard, J. G., and D'Souza-Schorey, C. (2001). An essential role for ARF6-regulated membrane traffic in adherens junction turnover and epithelial cell migration. EMBO J. *20*, 4973–4986.

Palacios, F., Schweitzer, J. K., Boshans, R. L., and D'Souza-Schorey, C. (2002). ARF6-GTP recruits Nm23-H1 to facilitate dynamin-mediated endocytosis during adherens junctions disassembly. Nat. Cell Biol. *4*, 929–936.

Pasquale, E. B. (2005). Eph receptor signalling casts a wide net on cell behaviour. Nat. Rev. Mol. Cell Biol. *6*, 462–475.

Pasquale, E. B. (2008). Eph-Ephrin bidirectional signaling in physiology and disease. Cell *133*, 38–52.

Penela, P., Ribas, C., Aymerich, I., Eijkelkamp, N., Barreiro, O., Heijnen, C. J., Kavelaars, A., Sanchez-Madrid, F., and Mayor, F., Jr. (2008). G protein-coupled receptor kinase 2 positively regulates epithelial cell migration. EMBO J. *27*, 1206–1218.

Phee, H., Abraham, R. T., and Weiss, A. (2005). Dynamic recruitment of PAK1 to the immunological synapse is mediated by PIX independently of SLP-76 and Vav1. Nat. Immunol. *6*, 608–617.

Premont, R. T., Claing, A., Vitale, N., Freeman, J. L., Pitcher, J. A., Patton, W. A., Moss, J., Vaughan, M., and Lefkowitz, R. J. (1998). β2-Adrenergic receptor regulation by GIT1, a G protein-coupled receptor kinase-associated ADP ribosylation factor GTPase-activating protein. Proc. Natl. Acad. Sci. USA *95*, 14082–14087.

Radhakrishna, H., Al Awar, O., Khachikian, Z., and Donaldson, J. G. (1999). ARF6 requirement for Rac ruffling suggests a role for membrane trafficking in cortical actin rearrangements. J. Cell Sci. *112*, 855–866.

Ruiz, J. C., and Robertson, E. J. (1994). The expression of the receptor-protein tyrosine kinase gene, eck, is highly restricted during early mouse development. Mech. Dev. *46*, 87–100.

Santy, L. C., and Casanova, J. E. (2001). Activation of ARF6 by ARNO stimulates epithelial cell migration through downstream activation of both Rac1 and phospholipase D. J. Cell Biol. *154*, 599–610.

Surawska, H., Ma, P. C., and Salgia, R. (2004). The role of ephrins and Eph receptors in cancer. Cytokine Growth Factor Rev. *15*, 419–433.

Suzuki, T., *et al.* (2006). Crucial role of the small GTPase ARF6 in hepatic cord formation during liver development. Mol. Cell. Biol. *26*, 6149–6156.

Tague, S. E., Muralidharan, V., and D'Souza-Schorey, C. (2004). ADP-ribosylation factor 6 regulates tumor cell invasion through the activation of the MEK/ERK signaling pathway. Proc. Natl. Acad. Sci. USA *101*, 9671–9676.

Takeichi, M. (1991). Cadherin cell adhesion receptors as a morphogenetic regulator. Science *251*, 1451–1455.

Totaro, A., Paris, S., Asperti, C., and de Curtis, I. (2007). Identification of an intramolecular interaction important for the regulation of GIT1 functions. Mol. Biol. Cell *18*, 5124–5138.

Vestweber, D., and Kemler, R. (1985). Identification of a putative cell adhesion domain of uvomorulin. EMBO J. *4*, 3393–3398.

Zantek, N. D., Azimi, M., Fedor-Chaiken, M., Wang, B., Brackenbury, R., and Kinch, M. S. (1999). E-cadherin regulates the function of the EphA2 receptor tyrosine kinase. Cell Growth Differ. *10*, 629–638.

Zelinski, D. P., Zantek, N. D., Stewart, J. C., Irizarry, A. R., and Kinch, M. S. (2001). EphA2 overexpression causes tumorigenesis of mammary epithelial cells. Cancer Res. *61*, 2301–2306.

Zhang, H., Webb, D. J., Asmussen, H., and Horwitz, A. F. (2003). Synapse formation is regulated by the signaling adaptor GIT1. J. Cell Biol. *161*, 131–142.

THE JOURNAL OF BIOLOGICAL CHEMISTRY VOL. 284, NO. 13, pp. 8548–8556, March 27, 2009

FBP17 Mediates a Common Molecular Step in the Formation of Podosomes and Phagocytic Cups in Macrophages*[S]

Received for publication, July 23, 2008, and in revised form, December 29, 2008 Published, JBC Papers in Press, January 20, 2009, DOI 10.1074/jbc.M805638200

Shigeru Tsuboi[‡1], Hidetoshi Takada[§], Toshiro Hara[§], Naoki Mochizuki[¶], Tomihisa Funyu[‖], Hisao Saitoh[‖], Yuriko Terayama[‖], Kanemitsu Yamaya[‖], Chikara Ohyama[**], Shigeaki Nonoyama[‡‡], and Hans D. Ochs[§§]

From the [‡]Infectious and Inflammatory Disease Center, Burnham Institute for Medical Research, La Jolla, California 92037, the [§]Department of Pediatrics, Graduate School of Medical Sciences, Kyushu University, Fukuoka 812-8582, Japan, the [¶]Department of Structural Analysis, National Cardiovascular Center Research Institute, Osaka 565-8565, Japan, the [‖]Oyokyo Kidney Research Institute, Hirosaki 036-8243, Japan, the [**]Department of Urology, Hirosaki University School of Medicine, Hirosaki 036-8562, Japan, the [‡‡]Department of Pediatrics, National Defense Medical College, Saitama 359-0042, Japan, and the [§§]Department of Pediatrics, Research Center for Immunity and Immunotherapy, Seattle Children's Hospital Research Institute, Seattle, Washington 98101

Macrophages act to protect the body against inflammation and infection by engaging in chemotaxis and phagocytosis. In chemotaxis, macrophages use an actin-based membrane structure, the podosome, to migrate to inflamed tissues. In phagocytosis, macrophages form another type of actin-based membrane structure, the phagocytic cup, to ingest foreign materials such as bacteria. The formation of these membrane structures is severely affected in macrophages from patients with Wiskott-Aldrich syndrome (WAS), an X chromosome-linked immunodeficiency disorder. WAS patients lack WAS protein (WASP), suggesting that WASP is required for the formation of podosomes and phagocytic cups. Here we have demonstrated that formin-binding protein 17 (FBP17) recruits WASP, WASP-interacting protein (WIP), and dynamin-2 to the plasma membrane and that this recruitment is necessary for the formation of podosomes and phagocytic cups. The N-terminal EFC (extended FER-CIP4 homology)/F-BAR (FER-CIP4 homology and Bin-amphiphysin-Rvs) domain of FBP17 was previously shown to have membrane binding and deformation activities. Our results suggest that FBP17 facilitates membrane deformation and actin polymerization to occur simultaneously at the same membrane sites, which mediates a common molecular step in the formation of podosomes and phagocytic cups. These results provide a potential mechanism underlying the recurrent infections in WAS patients.

Podosomes (see Fig. 1*A*) are micron-scale, dynamic, actin-based protrusions observed in motile cells such as macrophages, dendritic cells, osteoclasts, certain transformed fibroblasts, and carcinoma cells (1). Podosomes play an important role in macrophage chemotactic migration, which is critical for recruitment of leukocytes to inflamed tissues. Podosomes are both adhesion structures and the sites of extracellular matrix degradation (2). Adhesion to and degradation of the extracellular matrix are essential processes for the successful migration of macrophages in tissues. Podosomes occur in most macrophages and can be observed by differentiating human primary monocytes into macrophages with macrophage-colony stimulating factor-1 (M-CSF-1)[2] and staining the F-actin using phalloidin (3, 4). Podosomes labeled in this way appear as F-actin-rich dots (see Fig. 1*C*). Podosome formation has recently been directly observed *in vitro* and *in vivo* in leukocyte migration through the endothelium, diapedesis (5).

Phagocytosis of bacterial pathogens is one of the most important primary host defense mechanisms against infections. The phagocytic cup (see Fig. 1*B*) is an actin-based membrane structure formed at the plasma membrane of phagocytes, including macrophages, upon stimulation with foreign materials such as bacteria. The phagocytic cup captures and ingests foreign materials, and its formation is an essential first step in phagocytosis leading to the digestion of foreign materials (6, 7). When macrophages are stimulated by foreign materials, podosomes disappear, and phagocytic cups, which are also rich in F-actin, are formed to ingest the foreign materials (see Fig. 1*D*).

Wiskott-Aldrich syndrome (WAS) is an X chromosome-linked immunodeficiency disorder. Patients with WAS suffer from severe bleeding, eczema, recurrent infection, autoimmune diseases, and an increased risk of lymphoreticular malignancy (8–10). The causative gene underlying WAS encodes Wiskott-Aldrich syndrome protein (WASP) (11). WASP deficiency due to the mutation or deletion causes defects in adhesion, chemotaxis, phagocytosis, and the development of hematopoietic cells in WAS patients (10).

* This work was supported, in whole or in part, by National Institutes of Health Grant R01HD042752 (to S. T.). The costs of publication of this article were defrayed in part by the payment of page charges. This article must therefore be hereby marked "*advertisement*" in accordance with 18 U.S.C. Section 1734 solely to indicate this fact.

[S] The on-line version of this article (available at http://www.jbc.org) contains six supplemental figures.

[1] To whom correspondence should be addressed: Dept. of Biochemistry, Oyokyo Kidney Research Institute, 90 Yamazaki, Kozawa, Hirosaki 036-8243, Japan. Tel.: 81-172-87-1221; Fax: 81-172-87-1228; E-mail: tsuboi@oyokyo.jp.

[2] The abbreviations used are: M-CSF-1, macrophage-colony stimulating factor-1; FBP17, formin-binding protein 17; WAS, Wiskott-Aldrich syndrome; WASP, Wiskott-Aldrich syndrome protein; N-WASP, neuronal WASP; WIP, WASP interacting-protein; EFC domain, extended FER-CIP4 homology domain; F-BAR domain, FER-CIP4 homology and Bin-amphiphysin-Rvs domain; PMA, phorbol 12-myristate 13-acetate; GFP, green fluorescence protein; siRNA, short interfering RNA; FITC, fluorescein isothiocyanate; PDZ-GEF, PDZ-guanine nucleotide exchange factor; HEK293 cells, human embryonic kidney 293 cells; HA, hemagglutinin; SH3, src homology 3 domain; dSH3, SH3 domain deletion; GST, glutathione *S*-transferase; , $PI(4,5)P_2$, phosphatidylinositol 4,5-bisphosphate; siFBP, siRNA for FBP17; siC, scrambled control siRNA.

The formation of podosomes and phagocytic cups is severely affected in macrophages from WAS patients (3, 12, 42), suggesting that WASP is involved in the formation of these structures. However, the detailed molecular mechanisms of their formation remain unknown. WASP is complexed with a cellular WASP-interacting partner, WASP-interacting protein (WIP) (13, 14). Recently, two groups (including us) have demonstrated that WASP and WIP form a complex and that the WASP-WIP complex is required for the formation of podosomes (4, 15) and phagocytic cups (16). Here, we identified formin-binding protein 17 (FBP17) as a protein interacting with the WASP-WIP complex and examined the role of FBP17 in the formation of podosomes and phagocytic cups.

EXPERIMENTAL PROCEDURES

Reagents and Antibodies—Recombinant human macrophage-colony stimulating factor-1 (M-CSF-1) was purchased from R&D Systems (Minneapolis, MN). Phenylmethylsulfonyl fluoride, leupeptin, pepstain A, aprotinin, IGEPAL CA-630, paraformaldehyde, saponin, bovine serum albumin, 3-methyladenine, latex beads (3 μm in diameter), phorbol 12-myristate 13-acetate (PMA), human IgG, glycerol, Triton X-100, anti-FLAG monoclonal antibody (M2), and anti-β-actin antibody were purchased from Sigma-Aldrich. The anti-WASP monoclonal antibody, anti-WIP polyclonal antibody, and anti-Myc monoclonal antibody (9E10) were obtained from Santa Cruz Biotechnology Inc. (Santa Cruz, CA). The anti-dynamin-2 antibody was purchased from BD Biosciences. The rat anti-hemagglutinin (HA) monoclonal antibody (3F10) was purchased from Boehringer Ingelheim (Ridgefield, CT). The Cy2-labeled anti-rat IgG was obtained from Jackson ImmunoResearch Laboratories (West Grove, PA).

Yeast Two-hybrid Screening—We screened a human lymphocyte cDNA library (Origene Technology Inc., Rockville, MD) using a full-length WIP as bait. A cDNA encoding full-length WIP was cloned into pGilda (BD Biosciences Clontech). The EGY48 yeast strain was transformed with pGilda-WIP, the human lymphocyte cDNA library, and pSH18–34, a reporter plasmid for the β-galactosidase assay. Transformants were assayed for Leu prototrophy, and a filter assay was performed for β-galactosidase measurement (17).

Cells and Transfection—THP-1 and human embryonic kidney (HEK) 293 cells were purchased from the American Type Culture Collection (Manassas, VA) and cultured in RPMI1640 and Dulbecco's modified Eagle's high glucose medium (Invitrogen), respectively, both supplemented with 10% fetal bovine serum. For human primary monocyte isolation, 10–30 ml of peripheral blood was drawn from healthy volunteers and WAS patients after informed consent was obtained. Monocytes were prepared from peripheral blood samples (10–30 ml) using a monocyte isolation kit II (Miltenyi Biotech Inc., Auburn, CA). Transfection of THP-1 cells and monocytes was performed with a Nucleofector device using a cell line Nucleofector kit V and a human monocyte Nucleofector kit, respectively, according to the manufacturer's instructions (Amaxa Biosystems, Gaithersburg, MD). Transfection of HEK293 cells was performed using SuperFect transfection reagent (Qiagen, Valencia, CA). THP-1 cells and monocytes were co-transfected with the FBP17 constructs and a GFP-expressing plasmid, pmaxGFP (Amaxa Biosystems Inc.), as a transfection marker. The transfection efficiency measured using pmaxGFP was 40–50% for THP-1 cells and 10–20% for monocytes.

RNA Interference—A short interfering RNA (siRNA) for FBP17 and its scrambled control siRNA was synthesized by Dharmacon (Lafayette, CO). The targeting sequence was 5′-CCCACTTCATATGTCGAAGTCTGTT-3′ (18). THP-1 cells and monocytes were transfected with siRNA using a cell line Nucleofector kit V and a human monocyte Nucleofector kit, respectively, and a Nucleofector device. Cells were co-transfected with an fluorescein isothiocyanate (FITC)-conjugated control siRNA, BLOCK-IT (Invitrogen), as a transfection marker. The transfection efficiency measured using BLOCK-IT was 40–50% for THP-1 cells and 10–20% for monocytes.

Immunoprecipitation—For immunoprecipitation of WASP from THP-1 cells, 2×10^7 cells were lysed in buffer A (50 mM Tris-HCl, pH 7.5, 75 mM NaCl, 1% Triton X-100, 1 mM phenylmethylsulfonyl fluoride, 1 μg/ml leupeptin, 1 μg/ml pepstatin A, 1 μg/ml aprotinin). Lysates were centrifuged at 10,000 × *g* at 4 °C for 15 min. The supernatant was incubated with 2 μg/ml anti-WASP monoclonal antibody (Santa Cruz Biotechnology) at 4 °C for 2 h and then incubated with anti-mouse IgG agarose (Sigma). The resin binding the immune complex was washed three times with 0.5 ml of buffer B (50 mM Tris-HCl, pH 7.5, 10% glycerol, 0.1% Triton X-100), and the complex was eluted with 1× Laemmli's SDS-PAGE sample buffer. Eluted proteins were subjected to SDS-PAGE and analyzed by immunoblotting for WASP, WIP, and FBP17.

GST Pull-down Assay—Glutathione *S*-transferase (GST) and a fusion protein of GST and the src homology 3 (SH3) domain of FBP17 (548–609 amino acids) (GST-FSH3) were purified from *Escherichia coli* (XL-1B) extracts using glutathione-Sepharose-4B. HEK293 cells were transfected with the cDNAs of Myc- or FLAG-tagged protein and lysed in buffer A. Lysates from the transfected cells were incubated with the affinity matrices of GST alone or GST-FSH3 at 4 °C for 1 h. After a 1-h incubation, the matrices were washed five times with buffer A, and pull-down samples were analyzed by immunoblotting using anti-Myc or anti-FLAG antibody.

Immunofluorescence Microscopy—THP-1 cells and monocytes grown on coverslips were differentiated into macrophages by incubation with 12.5 ng/ml PMA (Sigma) and 20 ng/ml M-CSF-1 (R&D Systems), respectively, for 72 h. HEK293 cells were transfected with various cDNA constructs and then cultured on coverslips for 48 h. Cells were fixed with 4% (w/v) paraformaldehyde, permeabilized with 0.1% (w/v) saponin, and blocked with 1% (w/v) bovine serum albumin. Cells were stained with primary antibodies and Alexa Fluor 488- or Alexa Fluor 564-labeled secondary antibodies (Invitrogen). Cells were also stained with Alexa Fluor 568-labeled phalloidin (Invitrogen). Cell staining was examined under a fluorescence microscope (Zeiss Axioplan AR) or an MRC 1024 SP laser point scanning confocal microscope (Bio-Rad).

Assays for the Formation of Podosomes and Phagocytic Cups—The formation of podosomes and phagocytic cups was assayed by visualizing these actin-based membrane structures by F-actin staining as described previously (4, 16). Briefly, podosomes

in differentiated THP-1 cells or macrophages were visualized by F-actin staining with Alexa Fluor 568-phalloidin. To form phagocytic cups in differentiated THP-1 cells or macrophages, latex beads (3 μm, Sigma) were opsonized with 0.5 mg/ml human IgG (Sigma), and cells grown on coverslips were incubated with the IgG-opsonized latex beads at 37 °C for 10 min in the presence of 10 mM 3-methyladenine (Sigma) to stabilize the phagocytic cups (16). The phagocytic cups were then also visualized with Alexa Fluor 568-phalloidin. Cells were examined under a fluorescence microscope (Zeiss Axioplan AR).

Assays for Macrophage Migration and Phagocytosis—For the macrophage migration assay, human macrophages (2×10^5 cells) were plated onto chemotaxis membranes with 5-μm pores (Corning, Acton, MA) coated with 0.15% gelatin/phosphate-buffered saline placed within Boyden chamber inserts. M-CSF-1 was used as a chemoattractant and diluted in serum-containing RPMI 1640 medium in lower chambers. After a 4-h incubation, non-migrating cells were removed by gently wiping the upper surface of the filter. The filter was removed from the inserts using a razor blade and mounted onto glass plates, and the number of migrating cells was counted under a fluorescence microscope. For the phagocytosis assay, human macrophages (1×10^6 cells) were seeded on coverslips and incubated with 0.5 ml of RPMI 1640 medium containing IgG-opsonized latex beads (3 μm) at 4 °C for 10 min, allowing the beads to attach to cells. Phagocytosis was initiated by adding 1.5 ml of preheated RPMI 1640 medium, and the cells were incubated with the beads at 37 °C for 30 min. Control plates were incubated at 4 °C to estimate nonspecific binding of latex beads to the cells. After incubation, the cells were vigorously washed with phosphate-buffered saline, and the number of intracellular latex beads was determined by counting beads within cells under a fluorescence microscope. The percentage of phagocytosis was calculated as the total number of cells with at least one bead as a percentage of the total number of cells counted. At least 100 cells were examined.

Cell Fractionation—To prepare the cytoplasmic and membrane fractions, macrophages (1×10^6 cells) were washed with ice-cold phosphate-buffered saline and suspended in 50 mM Tris-HCl buffer, pH 7.5, containing 1 mM EDTA and proteinase inhibitors as described above. The cell suspensions were sonicated four times on ice for 5 s each using a bath-type sonicator followed by ultracentrifugation at 265,000 × *g* at 4 °C for 2 h. The supernatant was used as the cytosolic fraction, and the pellet was resuspended in 50 mM Tris-HCl, pH 7.5, containing 1 mM EDTA and used as the membrane fraction. Anti-Caspase-3 (Santa Cruz Biotechnology) and anti-sodium potassium ATPase antibodies (AbCam, Inc., Cambridge, MA) were used to determine the purity of the cytosolic and membrane fractions, respectively.

Statistics—Statistically significant differences were determined using the Student's *t* test. Differences were considered significant if $p < 0.05$.

RESULTS

FBP17 Binds to the WASP-WIP Complex and Dynamin-2 in Macrophages—To explore the detailed molecular mechanisms of the formation of podosomes and phagocytic cups, we searched for a protein interacting with the WASP-WIP complex. We identified FBP17 as a WIP-binding protein in a yeast two-hybrid screen using the full-length WIP as bait. FBP17 was originally identified as a protein binding to formin, a protein that regulates the actin cytoskeleton (19). FBP17 is a member of the *Schizosaccharomyces pombe* Cdc15 homology (PCH) protein family (20) and contains an N-terminal extended FER-CIP4 homology (EFC) domain (also known as the FER-CIP4 homology and Bin-amphiphysin-Rvs (F-BAR) domain), protein kinase C-related kinase homology region 1 (HR1), and an SH3 domain (Fig. 1*E*). The EFC/F-BAR domain has membrane binding and deformation activities, and FBP17 is involved in endocytosis in transfected COS-7 cells (18, 21, 22).

To confirm that FBP17 directly interacts with WIP or WASP, we performed GST pull-down assays using a fusion protein of GST and the SH3 domain of FBP17 (GST-FBPSH3). Purified GST and the GST-FSH3 fusion protein were subjected to SDS-PAGE (Fig. 1*F*, *lanes 1* and *2*). The HEK293 transfected cells express the Myc- and FLAG-tagged proteins (Fig. 1*F*, *lanes 3–6*). The results from the GST pull-down assays were shown (Fig. 1*F*, *lanes 7–14*). Both WASP and WIP were pulled down by GST-FSH3 (Fig. 1, *lanes 10* and *14*), indicating that the SH3 domain of FBP17 directly interacts with both proteins.

It has previously been shown that FBP17 binds to N-WASP and dynamin in transfected cells (18, 21). We examined whether FBP17 binds to WASP, WIP, and dynamin-2 in macrophages. THP-1 (human monocyte cell line) cells closely resemble monocyte-derived macrophages when differentiated by stimulation with PMA (23) and form podosomes and phagocytic cups that are morphologically and functionally indistinguishable from those in primary macrophages (supplemental Fig. 1) (4, 16, 23). WASP was immunoprecipitated from the lysates of PMA-differentiated THP-1 cells with an anti-WASP monoclonal antibody (Fig. 1*G*, *lanes 2*, *5*, and *8*) followed by immunoblotting using antibodies to FBP17 (21), WASP, and WIP. Both WIP and FBP17 co-immunoprecipitated with WASP (Fig. 1*G*, *lanes 5* and *8*). FBP17 also co-immunoprecipitated with dynamin-2 (Fig. 1*G*, *lanes 14*). These results, taken together with the results in Fig. 1*F*, suggest that FBP17 binds to the WASP-WIP complex and dynamin-2 in macrophages.

We next used immunofluorescence to examine whether FBP17 localizes at podosomes and phagocytic cups because the WASP-WIP complex is an essential component of podosomes (4, 15) and phagocytic cups (16). THP-1 cells transfected with FLAG-tagged FBP17 (FLAG-FBP17) and differentiated by stimulation with PMA were stained with an anti-FLAG monoclonal antibody to visualize FBP17 and with phalloidin to visualize the F-actin in podosomes and phagocytic cups (Fig. 1, *H* and *I*, *left* and *middle panels*). Merged images revealed that both F-actin and FBP17 are present in podosomes and phagocytic cups (Fig. 1, *H* and *I*, *right panels*), indicating that FBP17 localizes at podosomes and phagocytic cups.

Importance of FBP17 in the Formation of Podosomes and Phagocytic Cups—To determine the importance of FBP17 in the formation of podosomes and phagocytic cups, we knocked down FBP17 in THP-1 cells with siRNAs. To confirm that the expression of FBP17 was knocked down in cells, we transfected THP-1 cells with siRNAs, prepared lysates from the total

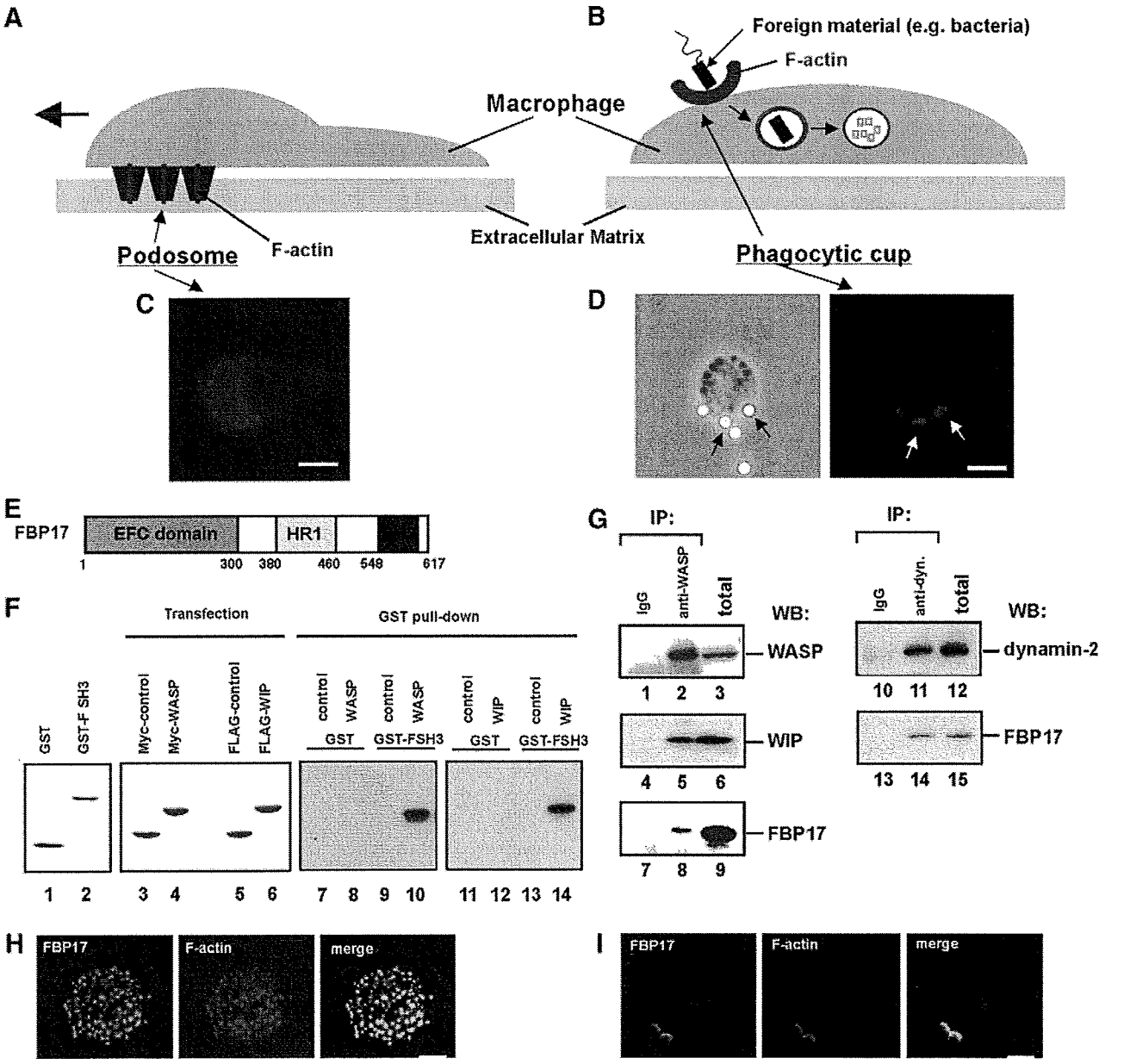

FIGURE 1. **FBP17 is a component of podosomes and phagocytic cups.** *A* and *B*, schematic drawings of podosomes (*A*) and a phagocytic cup (*B*) in macrophages. *C*, podosomes in macrophages were visualized by F-actin staining using Alexa Fluor 568-phalloidin. *D*, macrophages incubated with IgG-opsonized latex beads formed phagocytic cups to ingest the beads. A phase contrast image of a macrophage forming phagocytic cups (*left panel*). *Black arrows* indicate the latex beads ingested by the macrophage. Phagocytic cups were visualized by F-actin staining using Alexa Fluor 568-phalloidin (*right panel*). *White arrows* indicate the phagocytic cups. The *bar* is 10 μm. *E*, the domain organization of FBP17. *HR1*, protein kinase C-related kinase homology region 1. *F*, FBP17 interacts directly with WASP and WIP via its SH3 domain. GST and the GST-FBP17 SH3 domain fusion protein (GST-FSH3) were purified from bacteria extracts. Purified proteins were subjected to SDS-PAGE and stained with Coomassie Brilliant Blue (*lanes 1* and *2*). HEK293 cells were transfected with the cDNAs of Myc-tagged control protein (Myc-PDZ-GEF), Myc-WASP, FLAG-PDZ-GEF, or FLAG-WIP, and the expression of those proteins were analyzed by immunoblotting (*lanes 3–6*). Lysates from the HEK293 transfected cells were incubated with the affinity matrices of GST alone or GST-FSH3. Pull-down samples were analyzed by immunoblotting using anti-Myc antibody (*lanes 7–10*) and anti-FLAG antibody (*lanes 11–14*). *G*, FBP17 binds WASP, WIP, and dynamin-2. WASP was immunoprecipitated (*IP*) from the lysates of PMA-differentiated THP-1 cells with anti-WASP or a control IgG (*left panel, lanes 1–9*). The WASP immunoprecipitates and total lysates were analyzed by immunoblotting (*WB*) for WASP (*lanes 1–3*), WIP (*lanes 4–6*), and FBP17 (*lanes 7–9*). Dynamin was also immunoprecipitated from the THP-1 cell lysates with an anti-dynamin polyclonal antibody. The dynamin immunoprecipitates and total lysates were analyzed by immunoblotting for dynamin-2 (*lanes 10–12*) and FBP17 (*lanes 13–15*). *H* and *I*, confocal laser scanning micrographs of PMA-differentiated THP-1 cells. *H*, THP-1 cells transfected with FLAG-tagged FBP17 cDNA (FBP17) were double-stained with an anti-FLAG monoclonal antibody (*left panel*) and phalloidin (*center panel*) to visualize the F-actin in podosomes. *Yellow* indicates co-localization of FBP17 (*green*) and F-actin, podosomes (*red*) (*right panel*). *I*, THP-1 cells transfected with FLAG-FBP17 cDNA were incubated with IgG-opsonized latex beads and double-stained with anti-FLAG antibody and phalloidin. Phagocytic cups were visualized by F-actin staining (*center panel*). *Yellow* indicates co-localization of FBP17 (*green*) and F-actin, phagocytic cups (*red*) (*right panel*). The *bar* is 10 μm.

siRNAs-transfected cells, and analyzed the expression level of FBP17 by immunoblotting. THP-1 cells transfected with the siRNA for FBP17 expressed ~40% less FBP17 than cells transfected with a scrambled control siRNA based on the immunoblots (Fig. 2*A*, *lanes 1* and *2*) but expressed the same level of β-actin (Fig. 2*A*, *lanes 3* and *4*). The transfection efficiency of

Role of FBP17 in the Podosome and Phagocytic Cup Formation

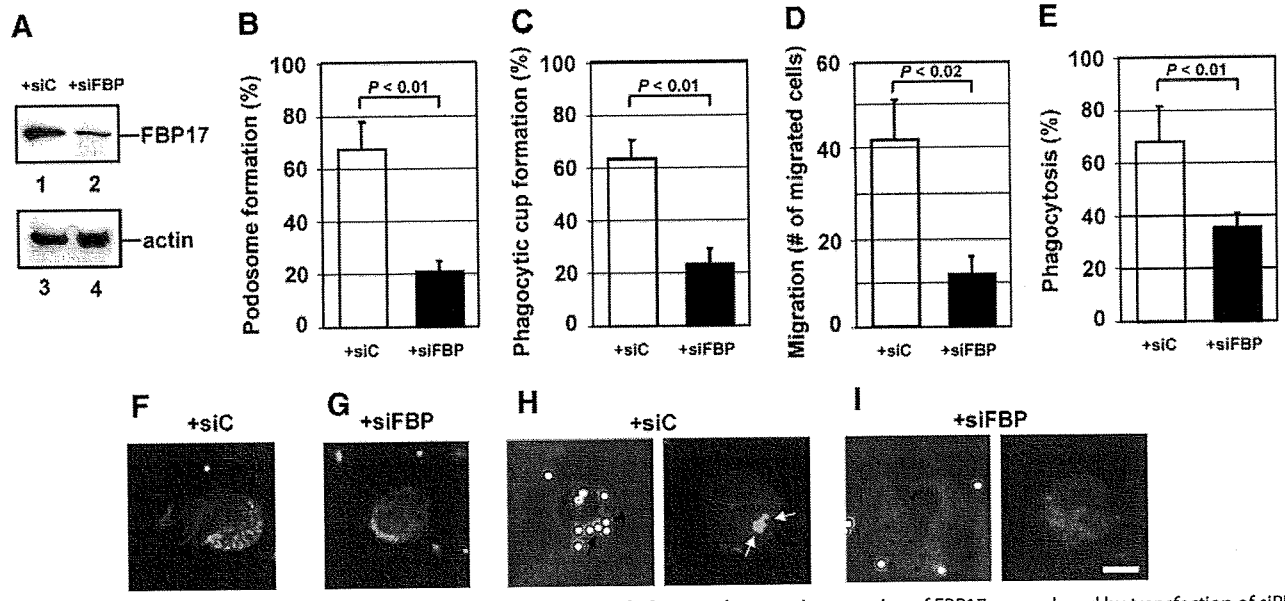

FIGURE 2. **The importance of FBP17 in the formation of podosomes and phagocytic cups.** *A*, expression of FBP17 was reduced by transfection of siRNA. THP-1 cells were transfected with siRNA for FBP17 (siFBP; *lanes 2* and *4*) or its scrambled control siRNA (siC; *lanes 1* and *3*). Lysates prepared from total transfected cells were analyzed by immunoblotting for FBP17 (*lanes 1* and *2*) and β-actin (*lanes 3* and *4*). *B* and *C*, effects of FBP17 siRNA on the formation of podosomes and phagocytic cups in macrophages. Human primary monocytes were co-transfected with siFBP (*closed bars*) or siC (*open bars*) and an FITC-conjugated control siRNA and then differentiated into macrophages with M-CSF-1. FITC-positive transfected cells were examined for the formation of podosomes (*B*) or phagocytic cups (*C*), and the percentage of cells with podosomes or phagocytic cups was scored. *D* and *E*, effects of FBP17 siRNA on the functions of podosomes and phagocytic cups. Macrophages co-transfected with siFBP (*closed bars*) or siC (*open bars*) and the FITC-conjugated control siRNA were assayed for macrophage migration (*D*) or phagocytosis of IgG-opsonized latex beads (*E*). Data represent the mean ± S.D. of triplicate experiments. *F–I*, immunofluorescence micrographs of a representative cell from each experiment. Cells transfected with siC (*F*) and siFBP (*G*) were stained with Alexa Fluor 568-phalloidin. Cells transfected with siC (*H*) or siFBP (*I*) were incubated with IgG-opsonized latex beads and then stained with phalloidin. The *left* and *right panels* are phase contrast and immunofluorescence micrographs, respectively. The *bar* is 10 μm.

THP-1 cells was estimated to be 40–50% from the expression of green fluorescent protein (GFP) used as a transfection control. Therefore, the decrease in FBP17 expression indicates that FBP17 was efficiently knocked down in most transfected cells.

Human primary monocytes were co-transfected with the FBP17 siRNAs and a FITC-conjugated control siRNA as a transfection marker. After differentiation of the monocytes into macrophages with M-CSF-1, FITC-positive cells were examined for the formation of podosomes and phagocytic cups. To quantify their formation, we scored the percentage of cells with podosomes or phagocytic cups among FITC-positive cells. When the expression of FBP17 was knocked down, the formation of both podosomes and phagocytic cups in macrophages was significantly reduced ($p < 0.01$; Fig. 2, *B* and *C*). These results suggest that FBP17 is necessary for the formation of podosomes and phagocytic cups. A representative cell from each experiment is shown in Fig. 2, *F* and *G*, for podosomes and in Fig. 2, *H* and *I*, for phagocytic cups. We then assayed macrophage migration as a podosome function and phagocytosis as a phagocytic cup function. When expression of FBP17 was knocked down, macrophage migration through a gelatin filter toward a chemoattractant was significantly reduced in cells transfected with FBP17 siRNA ($p < 0.02$; Fig. 2*D*). Phagocytosis of IgG-opsonized latex beads was also reduced (Fig. 2*E*). These results suggest that FBP17 is essential for chemotaxis and phagocytosis because of its role in forming podosomes and phagocytic cups, respectively.

FBP17 Recruits the WASP-WIP Complex to the Plasma Membrane—Recent biochemical analyses revealed that FBP17 binds to a membrane phospholipid, phosphatidylinositol 4,5-bisphosphate ($PI(4,5)P_2$), through its EFC/F-BAR domain and to N-WASP and dynamin via its SH3 domain (18, 21, 24). We have shown that although WASP and WIP are cytosolic proteins, the WASP-WIP complex localizes at podosomes and phagocytic cups (4, 16). We then examined whether FBP17 recruits the WASP-WIP complex to the plasma membrane in macrophages. We focused on the roles of the EFC and SH3 domains of FBP17 and constructed three FBP17 mutants for the recruitment experiments: a Lys-33 to Glu (K33E) substitution, a Lys-166 to Ala (K166A) substitution, and an SH3 domain deletion (dSH3). Both substitution mutations in the EFC domain (K33E and K166A) significantly reduce membrane binding and deformation (22), and the dSH3 mutant does not bind to WASP and WIP because the SH3 domain is the binding site of WASP and WIP (Fig. 1*F*). We co-transfected HEK293 cells with the FLAG-tagged FBP17 constructs, WASP, and WIP. A C-terminal fragment (1146–1429 amino acids) of PDZ-GDP exchange factor (PDZ-GEF) was used as a negative control for FBP17 because this fragment is stable in the cytosol and does not interact with any WASP-related proteins (4, 16, 25). We confirmed the expression of FBP17 and its mutants in cells by immunoblotting (supplemental Fig. 2) and immunoprecipitated FLAG-tagged proteins from lysates of the transfected cells with anti-FLAG antibody (Fig. 3*A*, *lanes 1–5*). WASP and WIP were detected in the immunoprecipitates from cells

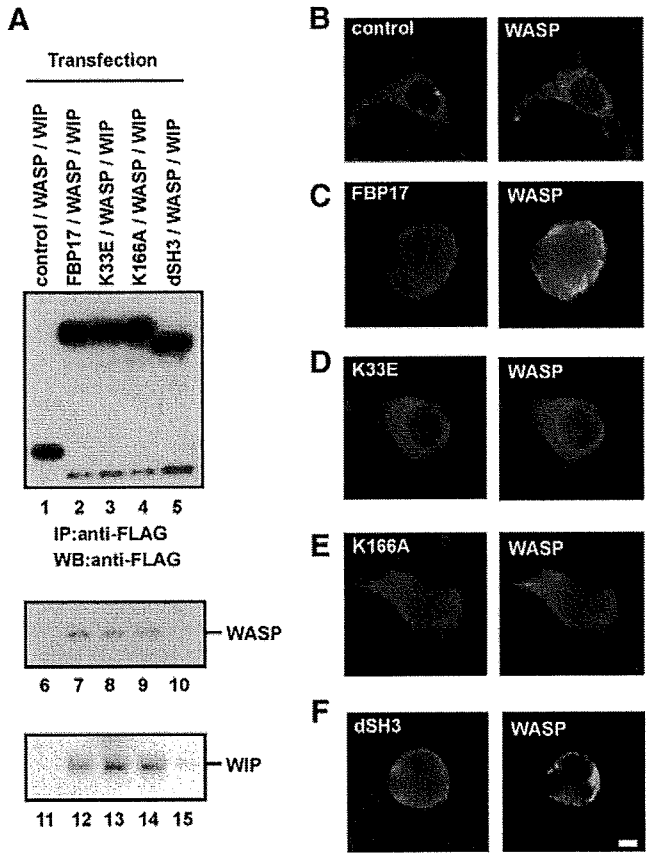

FIGURE 3. **FBP17 recruits WASP, WIP, and dynamin-2 to the plasma membrane.** *A*, HEK293 cells were co-transfected with cDNAs of the indicated FLAG-tagged proteins, Myc-tagged WASP, and HA-tagged WIP. The FLAG-tagged proteins were immunoprecipitated (*IP*) from lysates of the transfected cells with an anti-FLAG antibody followed by immunoblotting (*WB*) using antibodies to FLAG (*lanes 1–5*), WASP (*lanes 6–10*), and WIP (*lanes 11–15*). *B–F*, transfected HEK293 cells expressing FLAG-tagged proteins, Myc-WASP, and HA-WIP were double-stained with an anti-FLAG antibody and anti-WASP antibody. *B–F*, cells expressing FLAG-PDZ-GEF (*B*), FLAG-FBP17 (*C*), the FLAG-tagged FBP17 mutant with the K33E missense mutation (*D*), K166A (*E*), and the SH3-deleted FBP17 mutant dSH3 (*F*). The *bar* is 10 μm.

expressing the FLAG-tagged FBP17, K33E, and K166A constructs (Fig. 3*A*, *lanes 7–9* and *12–14*) but not the FLAG-tagged PDZ-GEF and dSH3 constructs (Fig. 3*A*, *lanes 6*, *10*, *11*, and *15*), indicating that FBP17 and its mutants K33E and K166A form a complex with WASP and WIP but that dSH3 not.

Next, cells expressing the FLAG-tagged proteins, WASP, and WIP were examined under the immunofluorescence microscope for the localization of the FLAG-tagged proteins and WASP. WASP and WIP were localized in the cytosol in cells transfected with only the WASP cDNA and only the WIP cDNA, respectively, as well as in cells expressing both WASP and WIP (supplemental Fig. 3). In cells co-expressing FLAG-PDZ-GEF (control) with WASP and WIP, both FLAG-PDZ-GEF and WASP were cytosolic (Fig. 3*B*). In cells co-expressing FLAG-FBP17 with WASP and WIP, FLAG-FBP17 localized at the plasma membrane because its EFC domain binds to the plasma membrane (Fig. 3*C*, *left panel*). In those cells, WASP also localized at the plasma membrane (Fig. 3*C*, *right panel*), indicating that FBP17 shifted the localization of WASP from the cytosol to the plasma membrane (Fig. 3, *B* and *C*). To confirm that the WASP-WIP complex was recruited to the plasma membrane, cells co-expressing FLAG-FBP17 with WASP and HA-tagged WIP were stained with an anti-FLAG monoclonal antibody and an anti-WASP polyclonal antibody or an anti-HA rat monoclonal antibody. Double staining revealed that both WASP and WIP co-localized with FLAG-FBP17 at the plasma membrane (supplemental Fig. 4, *A* and *B*). To further confirm the localization of the FBP17 mutants, cells co-expressing the FLAG-tagged FBP mutants, WASP, and WIP were stained with anti-FLAG monoclonal antibody. The K33E and K166A mutants were cytosolic and the SH3-deleted FBP17 mutant localized at the plasma membrane (supplemental Fig. 4*C*).

To determine the roles of the EFC and SH3 domains of FBP17 in this recruitment, we examined the localization of the FBP17 mutants and WASP in cells co-expressing the FBP mutants with WASP and WIP. Membrane tubulation in cells transfected with an FBP17 cDNA is an indicator of the membrane binding and deformation activities of FBP17 (18, 22). We detected *in vivo* membrane tubulation in cells expressing FBP17 and dSH3 but not in cells expressing K33E and K166A (supplemental Fig. 5). In cells co-expressing either FBP17 mutant (K33E or K166A) with WASP and WIP, both K33E and K166A were cytosolic (Fig. 3, *D* and *E*, *left panels*), and WASP was also cytosolic (Fig. 3, *D* and *E*, *right panels*). These results indicate that K33E and K166A are unable to recruit WASP to the plasma membrane, consistent with the inability of K33E and K166A to bind and deform the plasma membrane (supplemental Fig. 5).

The SH3-deleted FBP17 mutant, dSH3, localized at the plasma membrane (Fig. 3*F*, *left panel*) because its EFC domain is intact. However, WASP was cytosolic in cells co-expressing dSH3 with WASP and WIP (Fig. 3*F*, *right panel*), consistent with the inability of the dSH3 mutant to bind to WASP and WIP (Fig. 3*A*, *lanes 5*, *10*, and *15*).

To quantify the recruitment, we scored the percentage of cells in which WASP and WIP were localized at the plasma membrane. Cells expressing the FBP17 mutants (K33E, K166A, or dSH3) exhibited significantly lower plasma membrane localization of WASP and WIP than cells expressing FBP17 ($p < 0.05$; supplemental Fig. 6, *A* and *B*). FBP17 also recruited dynamin-2 to the plasma membrane, and both EFC and SH3 domains are necessary for this recruitment (supplemental Fig. 6*C*), as reported previously (18, 21). To confirm the localization of FBP17 and its mutants in cells co-expressing FBP17 with WASP, WIP, and dynamin-2, the transfected cells were stained with anti-FLAG monoclonal antibody. The wild-type FBP17 and dSH3 localized at the plasma membrane and the FLAG-PDZ-GEF (control) and the FBP mutants (K33E and K166A) were cytosolic (supplemental Fig. 6*D*).

Subcellular Localization of FBP17, WASP, WIP, and Dynamin-2 in Macrophages—To determine whether WASP, WIP, and dynamin-2 are recruited to the plasma membrane in macrophages when podosomes and phagocytic cups are formed, we examined the subcellular localization of FBP17, WASP, WIP, and dynamin-2 in macrophages forming podosomes or phagocytic cups. The cytosolic and membrane fractions were prepared from macrophages and analyzed by immunoblotting. Caspase-3 is a cytosolic marker, and sodium

potassium ATPase is a plasma membrane marker (26). FBP17 was detected in the membrane fraction from macrophages forming podosomes (Fig. 4*A*, *lane 9*). WASP, WIP, and dynamin-2 were also detected in the membrane fraction, although they are cytosolic proteins (Fig. 4*A*, *lanes 12, 15,* and *18*). FBP17 was detected in the membrane fraction from macrophages forming phagocytic cups (Fig. 4*B*, *lane 9*). WASP, WIP, and dynamin-2 were also detected in the membrane fractions from macrophages forming phagocytic cups (Fig. 4*B*, *lanes 12, 15,* and *18*). These results, taken together with Fig. 3, suggest that FBP17 recruits the WASP-WIP complex and dynamin-2 to the plasma membrane in macrophages and that both the EFC and the SH3 domains are necessary for this recruitment.

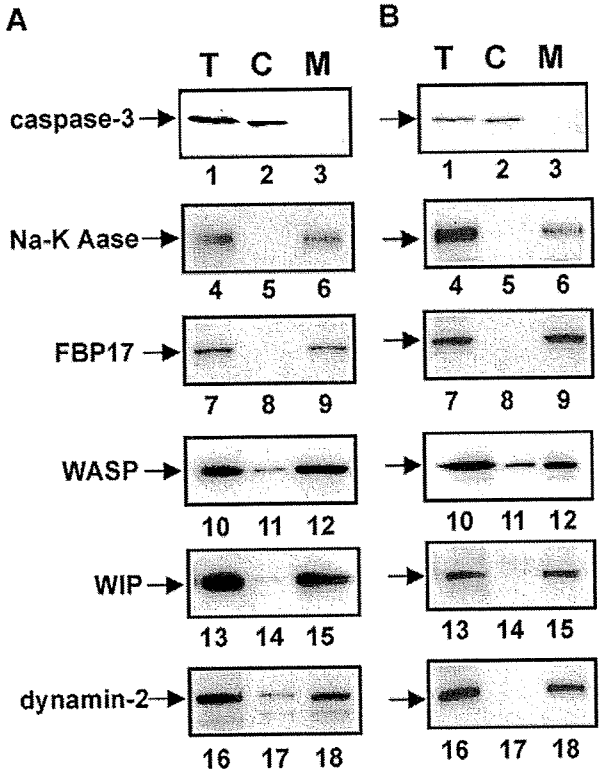

FIGURE 4. **Subcellular localization of FBP17, WASP, WIP, and dynamin-2 in macrophages.** *A*, macrophages forming podosomes. *B*, macrophages forming phagocytic cups. Total lysates (*T*), the cytosolic fraction (C), and the membrane fraction (*M*) prepared from macrophages forming podosomes (*A*) or phagocytic cups (*B*) were analyzed by immunoblotting for caspase-3 (*lanes 1–3*), sodium potassium ATPase (*Na-K Aase*; *lanes 4–6*), FBP17 (*lanes 7–9*), WASP (*lanes 10–12*), WIP (*lanes 13–15*), and dynamin-2 (*lanes 16–18*). Caspase-3 and sodium potassium ATPase (Na-K ATPase) are markers for the cytosol and plasma membrane, respectively.

The Role of Each Domain of FBP17 in the Formation of Podosomes and Phagocytic Cups—To determine the roles of the EFC and SH3 domains in the formation of podosomes and phagocytic cups, we examined whether overexpression of the FBP17 mutants affects the formation of these structures. We transfected THP-1 cells with the FBP17 constructs and confirmed the expression of FBP17 or the FBP17 mutants in transfected THP-1 cells by immunoblotting (Fig. 5*A*). When THP-1 cells were differentiated to obtain macrophage phenotypes with PMA, podosome formation was significantly reduced in cells overexpressing the K33E, K166A, and dSH3 FBP17 mutants when compared with the FBP17 wild type ($p < 0.01$; Fig. 5*B*). Phagocytic cup formation was also reduced in cells overexpressing the FBP17 mutants (Fig. 5*C*). These results indicate that the EFC domain and SH3 domain are essential for the formation of podosomes and phagocytic cups in macrophages.

Defects in Macrophages from WAS Patients—Our results suggest that the complex formation of FBP17 with WASP, WIP, and dynamin-2 at the plasma membrane is a critical step in the formation of podosomes and phagocytic cups (Figs. 1*G*, 3, and 4). In macrophages from WASP-deficient WAS patients, the complex does not form properly due to a lack of WASP expression. We examined macrophages from WASP-deficient WAS patients for the formation of podosomes and phagocytic cups. Two genetically independent WAS patients (WAS1, 211delT; and WAS2, 41–45delG) (27, 28) were assayed for the formation of those structures. Podosomes were completely absent (Fig. 6, *A–C*), and phagocytic cup formation was severely impaired (Fig. 6, *D–F*) in macrophages from both WAS patients, although FBP17, WIP, and dynamin-2 were expressed at the same level in patients as in normal individuals (Fig. 6*G*). In fact, the formation of podosomes and phagocytic cups was impaired in macrophages when the expression of WASP was reduced by siRNA transfection (4, 16). This is the first result showing that both podosome and phagocytic cup formations are defective in macrophages from WASP-deficient patients. These results are consistent with the previous observations (3, 12).

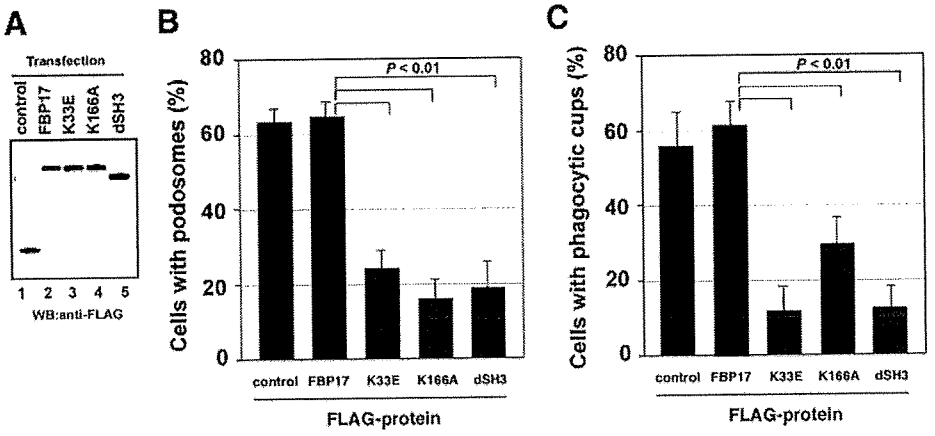

FIGURE 5. **The role of the EFC and SH3 domains of FBP17 in the formation of podosomes and phagocytic cups.** *A*, expression of FLAG-tagged proteins in transfected THP-1 cells. Total lysates prepared from transfected THP-1 cells were analyzed by immunoblotting (*WB*) using an anti-FLAG antibody. All of the FLAG-tagged proteins, FLAG-PDZ-GEF (control, *lane 1*), FLAG-FBP17 (*lane 2*), and the FBP17 mutants, K33E, K166A, and dSH3 (*lanes 3–5*) were expressed in THP-1 cells at similar levels. *B* and *C*, THP-1 cells co-transfected with cDNAs for the FLAG-tagged proteins and pmaxGFP were differentiated with PMA and then assayed for the formation of podosomes (*B*) and phagocytic cups (*C*). The percentage of cells with podosomes or phagocytic cups among all GFP-positive cells was scored. Data represent the mean ± S.D. of triplicate experiments.

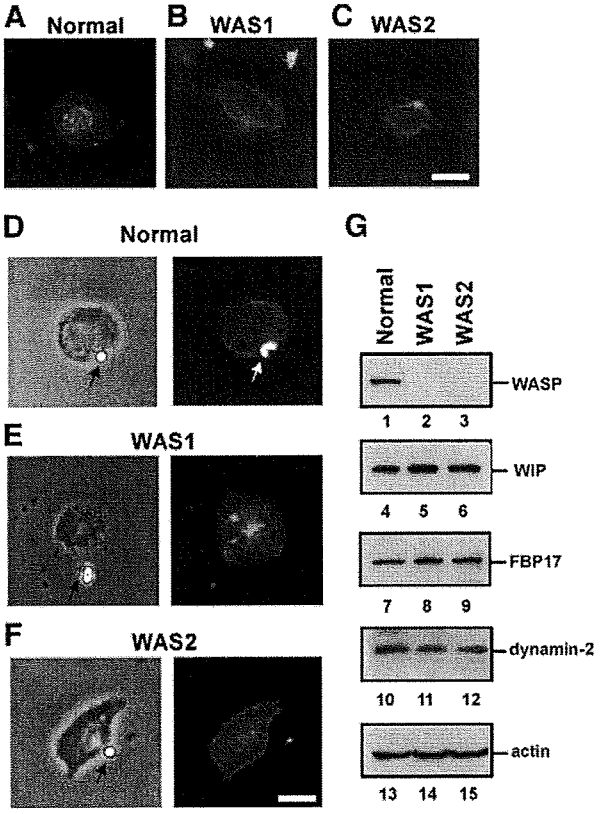

FIGURE 6. **Defective formation of podosomes and phagocytic cups in macrophages from WAS patients.** *A–F*, macrophages from a normal control and two genetically independent WAS patients (WAS1 and WAS2) were examined for the formation of podosomes (*A–C*) and phagocytic cups (*D–F*). The patients, WAS1 and WAS2, have the deletion mutations 211delT and 41–45delG, respectively, in their genomic DNAs. The *bars* are 10 μm. *G*, expression levels of WASP, WIP, FBP17, dynamin-2, and β-actin in WAS patients. Lysates prepared from macrophages from a normal control and two WAS patients (WAS1 and WAS2) were subjected to immunoblotting. WASP was not detected in the lysates from these WAS patients (*lanes 2* and *3*). Podosomes were completely absent (*A–C*) and phagocytic cup formation was severely impaired (*D–F*) in macrophages from both WAS patients, although FBP17, WIP, and dynamin-2 were expressed at the same level in patients as in normal individuals (*G*) (*lanes 4–12*).

These results give us a natural example that supports the importance of the complex formation of FBP17 with WASP, WIP, and dynamin-2 for the formation of podosomes and phagocytic cups.

DISCUSSION

Cell biological and structural analyses of the EFC domain of FBP17 have shown that the EFC domain binds to and deforms the plasma membrane (18, 22). It has previously been shown that the SH3 domain of FBP17 binds to N-WASP and dynamin in transfected cells (18, 21). However, physiologically important processes to which those activities of FBP17 contribute were unknown. Here, we have demonstrated that FBP17 recruits the WASP-WIP complex from the cytosol to the plasma membrane and that this recruitment is necessary for the formation of podosomes and phagocytic cups in macrophages. Our results suggest that FBP17 facilitates membrane deformation and actin polymerization induced by the WASP-WIP complex to occur simultaneously at the same membrane sites and that both are required for the formation of podosomes and phagocytic cups. This is supported by the observations that regulated actin polymerization is an essential process for the formation of podosomes (3) and phagocytic cups (29). Thus, FBP17 mediates a common molecular step in the formation of podosomes and phagocytic cups.

Macrophages have the ability to form both podosomes and phagocytic cups (Fig. 1, *A–D*). When macrophages having podosomes are stimulated with IgG-opsonized latex beads, the podosomes immediately disappear, and the phagocytic cups are formed at the site that the IgG beads attach. This observation indicates that the transition of the membrane structures occurs from podosomes to phagocytic cups. Macrophages migrate to sites of inflammation where they phagocytose pathogenic microbes and damaged tissue compounds and mediate local effector functions. Once macrophages encounter those materials at the site of inflammation, they stop migrating and phagocytose those materials. The transition of the macrophage functions occur from migration to phagocytosis. Podosomes and phagocytic cups are the essential membrane structures for migration and phagocytosis, respectively. Thus, the transition of the membrane structures from podosomes to phagocytic cups is essential and significant for the transition of the macrophage functions. Recently, two reports suggest that macrophage migration and phagocytosis include a common molecular mechanism to regulate actin cytoskeleton (40, 41). In this study, we identified a critical common molecular step mediated by FBP17 for the formation of podosomes and phagocytic cups, which are essential for migration and phagocytosis, respectively. In the future, elucidation of the molecular mechanisms underlying the transition would be intriguing.

It has been reported that dynamin-2 is also required for the formation of podosomes in transformed cells and osteoclasts (30–32) and phagocytic cups in a mouse macrophage cell line (33, 34) and that the FBP17-dynamin complex regulates the plasma membrane invagination (35). Our results suggest that FBP17 recruits dynamin-2 to the same site as membrane deformation and that this recruitment is also necessary for the formation of these structures (Figs. 3–5 and supplemental Fig. 6*C*). The formation of podosomes and phagocytic cups involves the process of the membrane protrusion (Fig. 1, *A–D*). The membrane protrusion requires the delivery of new membrane material (2). Our results, taken together with the above observations, suggest that dynamin-2 recruited by FBP17 to the plasma membrane probably plays an essential role in the formation of podosomes and phagocytic cups by regulating the recruitment of vesicles to the plasma membrane as new membrane material in macrophages.

Recently, the EFC domain of FBP17 was shown to bind strongly to the $PI(4,5)P_2$ (18, 22). On the other hand, it has been shown that $PI(4,5)P_2$ localizes at the podosomes in osteoclasts (36) and phagocytic cups (37, 38). These observations suggest that $PI(4,5)P_2$ is synthesized upon stimulation at the plasma membrane and plays an important role in the recruitment of FBP17 to the plasma membrane. Presumably, the $PI(4,5)P_2$ binding activity of the EFC domain is necessary for the localization of FBP17, and therefore, of the WASP-WIP complex and dynamin-2, at the sites where podosomes and phagocytic cups will form.

We suggest that the complex formation of FBP17 with WASP, WIP, and dynamin-2 at the plasma membrane is critical for the formation of podosomes and phagocytic cups (Figs. 1*G* and 3–5). In macrophages from WASP-deficient WAS patients, defects in the complex formation of FBP17 with WASP, WIP, and dynamin-2 impair the formation of podosomes and phagocytic cups (WAS1: 211delT (27); WAS2: 41–45delG(28) in Fig. 6), thereby reducing chemotaxis and phagocytosis by macrophages, which in turn would decrease the ability of host defense. The severity of WAS-associated symptoms was estimated and expressed as a score of 1–5. A score of 1 was assigned to patients with only thrombocytopenia and small platelets, and a score of 2 was assigned to patients with additional findings of mild, transient eczema or minor infections. Those with treatment-resistant eczema and recurrent infections despite optimal treatment received a score of 3 (mild WAS) or 4 (severe WAS). Regardless of the original score, if any patients then had autoimmune disease or malignancy, the score was changed to 5. The patients, WAS1 and WAS2, receive scores of 5 and 4, respectively. Both patients have the recurrent infections. We suggest that defective formation of podosomes and phagocytic cups in their macrophages (Fig. 6, *A–F*) reduces chemotaxis and phagocytosis, which are the critical processes to protect the body against infection, resulting in the recurrent infections. In addition, defective phagocytosis reduces the clearance of self-antigens such as apoptotic cells. This may cause the autoimmune diseases seen in WAS patients. In fact, Cohen *et al.* (39) recently reported that reduced clearance of apoptotic cells resulted in development of autoimmunity. Our findings therefore provide a potential mechanism for the recurrent infections and autoimmune diseases seen in WAS patients.

Acknowledgments—We thank Drs. M. Fukuda, R. C. Liddington, S. Courtneidge, A. Strongin (Burnham Institute for Medical Research), S. Grinstein (Hospital for Sich Children, Ontario, Canada), J. Condeelis (Albert Einstein Medical College), and P. De Camilli (Yale University) for critical reading of the manuscript and helpful discussion.

REFERENCES

1. Linder, S., and Aepfelbacher, M. (2003) *Trends Cell Biol.* **13,** 376–385
2. Linder, S. (2007) *Trends Cell Biol.* **17,** 107–117
3. Linder, S., Nelson, D., Weiss, M., and Aepfelbacher, M. (1999) *Proc. Natl. Acad. Sci. U. S. A.* **96,** 9648–9653
4. Tsuboi, S. (2007) *J. Immunol.* **178,** 2987–2995
5. Carman, C. V., Sage, P. T., Sciuto, T. E., Fuente, M. A. d. l., Geha, R. S., Ochs, H. D., Dvorak, H. F., Dvorak, A. M., and Springer, T. A. (2007) *Immunity* **26,** 784–797
6. Underhill, D. M., and Ozinsky, A. (2002) *Annu. Rev. Immunol.* **20,** 825–852
7. Leverrier, Y., and Ridley, A. J. (2001) *Curr. Biol.* **11,** 195–199
8. Wiskott, A. (1937) *Monatsschr. Kinderheilkd.* **68,** 212–216
9. Aldrich, R. A., Steinberg, A. G., and Campbell, D. C. (1954) *Pediatrics* **13,** 133–139
10. Notarangelo, L. D., Miao, C. H., and Ochs, H. D. (2008) *Curr. Opin. Hematol.* **15,** 30–36
11. Derry, J. M., Ochs, H. D., and Francke, U. (1994) *Cell* **78,** 635–644; Correction (1994) *Cell* **79,** 922
12. Lorenzi, R., Brickell, P. M., Katz, D. R., Kinnon, C., and Thrasher, A. J. (2000) *Blood* **95,** 2943–2946
13. Ramesh, N., Anton, I. M., Hartwig, J. H., and Geha, R. S. (1997) *Proc. Natl. Acad. Sci. U. S. A.* **94,** 14671–14676
14. Anton, I. M., de la Fuente, M. A., Sims, T. N., Freeman, S., Ramesh, N., Hartwig, J. H., Dustin, M. L., and Geha, R. S. (2002) *Immunity* **16,** 193–204
15. Chou, H. C., Anton, I. M., Holt, M. R., Curcio, C., Lanzardo, S., Worth, A., Burns, S., Thrasher, A. J., Jones, G. E., and Calle, Y. (2006) *Curr. Biol.* **16,** 2337–2344
16. Tsuboi, S., and Meerloo, J. (2007) *J. Biol. Chem.* **282,** 34194–34203
17. Tsuboi, S., Nonoyama, S., and Ochs, H. D. (2006) *EMBO Rep.* **7,** 506–511
18. Tsujita, K., Suetsugu, S., Sasaki, N., Furutani, M., Oikawa, T., and Takenawa, T. (2006) *J. Cell Biol.* **172,** 269–279
19. Chan, D. C., Bedford, M. T., and Leder, P. (1996) *EMBO J.* **15,** 1045–1054
20. Ho, H. Y., Rohatgi, R., Lebensohn, A. M., Le, M., Li, J., Gygi, S. P., and Kirschner, M. W. (2004) *Cell* **118,** 203–216
21. Kamioka, Y., Fukuhara, S., Sawa, H., Nagashima, K., Masuda, M., Matsuda, M., and Mochizuki, N. (2004) *J. Biol. Chem.* **279,** 40091–40099
22. Shimada, A., Niwa, H., Tsujita, K., Suetsugu, S., Nitta, K., Hanawa-Suetsugu, K., Akasaka, R., Nishino, Y., Toyama, M., Chen, L., Liu, Z. J., Wang, B. C., Yamamoto, M., Terada, T., Miyazawa, A., Tanaka, A., Sugano, S., Shirouzu, M., Nagayama, K., Takenawa, T., and Yokoyama, S. (2007) *Cell* **129,** 761–772
23. Auwerx, J. (1991) *Experientia (Basel)* **47,** 22–31
24. Kakimoto, T., Katoh, H., and Negishi, M. (2006) *J. Biol. Chem.* **281,** 29042–29053
25. Rebhun, J. F., Castro, A. F., and Quilliam, L. A. (2000) *J. Biol. Chem.* **275,** 34901–34908
26. Takayama, S., Krajewski, S., Krajewska, M., Kitada, S., Zapata, J. M., Kochel, K., Knee, D., Scudiero, D., Tudor, G., Miller, G. J., Miyashita, T., Yamada, M., and Reed, J. C. (1998) *Cancer Res.* **58,** 3116–3131
27. Jin, Y., Mazza, C., Christie, J. R., Giliani, S., Fiorini, M., Mella, P., Gandellini, F., Stewart, D. M., Zhu, Q., Nelson, D. L., Notarangelo, L. D., and Ochs, H. D. (2004) *Blood* **104,** 4010–4019
28. Imai, K., Morio, T., Zhu, Y., Jin, Y., Itoh, S., Kajiwara, M., Yata, J., Mizutani, S., Ochs, H. D., and Nonoyama, S. (2004) *Blood* **103,** 456–464
29. May, R. C., Caron, E., Hall, A., and Machesky, L. M. (2000) *Nat. Cell Biol.* **2,** 246–248
30. Ochoa, G. C., Slepnev, V. I., Neff, L., Ringstad, N., Takei, K., Daniell, L., Kim, W., Cao, H., McNiven, M., Baron, R., and De Camilli, P. (2000) *J. Cell Biol.* **150,** 377–389
31. McNiven, M. A., Baldassarre, M., and Buccione, R. (2004) *Front. Biosci.* **9,** 1944–1953
32. Bruzzaniti, A., Neff, L., Sanjay, A., Horne, W. C., De Camilli, P., and Baron, R. (2005) *Mol. Biol. Cell* **16,** 3301–3313
33. Gold, E. S., Underhill, D. M., Morrissette, N. S., Guo, J., McNiven, M. A., and Aderem, A. (1999) *J. Exp. Med.* **190,** 1849–1856
34. Tse, S. M., Furuya, W., Gold, E., Schreiber, A. D., Sandvig, K., Inman, R. D., and Grinstein, S. (2003) *J. Biol. Chem.* **278,** 3331–3338
35. Itoh, T., Erdmann, K. S., Roux, A., Habermann, B., Werner, H., and De Camilli, P. (2005) *Dev. Cell* **9,** 791–804
36. Chellaiah, M. A. (2005) *J. Biol. Chem.* **280,** 32930–32943
37. Botelho, R. J., Teruel, M., Dierckman, R., Anderson, R., Wells, A., York, J. D., Meyer, T., and Grinstein, S. (2000) *J. Cell Biol.* **151,** 1353–1368
38. Dewitt, S., Tian, W., and Hallett, M. B. (2006) *J. Cell Sci.* **119,** 443–451
39. Cohen, P. L., Caricchio, R., Abraham, V., Camenisch, T. D., Jennette, J. C., Roubey, R. A., Earp, H. S., Matsushima, G., and Reap, E. A. (2002) *J. Exp. Med.* **196,** 135–140
40. Brandt, D. T., Marion, S., Griffiths, G., Watanabe, T., Kaibuchi, K., and Grosse, R. (2007) *J. Cell Biol.* **178,** 193–200
41. Kato, M., Khan, S., d'Aniello, E., McDonald, K. J., and Hart, D. N. J. (2007) *J. Immunol.* **179,** 6052–6063
42. Calle, Y., Anton, I. M., Thrasher, A. J., and Jones, G. E. (2008) *J. Microsc. (Oxf.)* **231,** 494–505

THE JOURNAL OF BIOLOGICAL CHEMISTRY VOL. 284, NO. 9, pp. 5592–5601, February 27, 2009
Printed in the U.S.A.

Angiopoietin-1 Induces Krüppel-like Factor 2 Expression through a Phosphoinositide 3-Kinase/AKT-dependent Activation of Myocyte Enhancer Factor 2*[S]♦

Received for publication, September 8, 2008, and in revised form, November 24, 2008 Published, JBC Papers in Press, December 23, 2008, DOI 10.1074/jbc.M806928200

Keisuke Sako[‡], Shigetomo Fukuhara[‡1], Takashi Minami[§], Takao Hamakubo[§], Haihua Song[§], Tatsuhiko Kodama[§], Akiyoshi Fukamizu[¶], J. Silvio Gutkind[‖], Gou Young Koh[**], and Naoki Mochizuki[‡]

From the [‡]Department of Structural Analysis, National Cardiovascular Center Research Institute, 5-7-1 Fujishirodai, Suita, Osaka 565-8565, Japan, the [§]Laboratory for System Biology and Medicine, Research Center for Advanced Science and Technology, University of Tokyo, 4-6-1, Komaba, Meguro, Tokyo 153-8904, Japan, the [¶]Center for Tsukuba Advanced Research Alliance, University of Tsukuba, Tsukuba, Ibaraki 305-8577, Japan, the [‖]Oral and Pharyngeal Cancer Branch, NIDCR, National Institutes of Health, Bethesda, Maryland 20892, and the [**]Biomedical Research Center and Department of Biological Sciences, Korea Advanced Institute of Science and Technology, Guseong-dong, Daejeon 305-701, Korea

Angiopoietin-1 (Ang1) regulates both vascular quiescence and angiogenesis through the receptor tyrosine kinase Tie2. We and another group have recently shown that Ang1 and Tie2 form distinct signaling complexes at cell-cell and cell-matrix contacts and further demonstrated that the former selectively induces expression of Krüppel-like factor 2 (KLF2), a transcription factor involved in vascular quiescence. Here, we investigated the mechanism of how Ang1/Tie2 signal induces KLF2 expression to clarify the role of KLF2 in Ang1/Tie2 signal-mediated vascular quiescence. Ang1 stimulated KLF2 promoter-driven reporter gene expression in endothelial cells, whereas it failed when a myocyte enhancer factor 2 (MEF2)-binding site of KLF2 promoter was mutated. Depletion of MEF2 by siRNAs abolished Ang1-induced KLF2 expression, indicating the requirement of MEF2 in KLF2 induction by Ang1. Constitutive active phosphoinositide 3-kinase (PI3K) and AKT increased the MEF2-dependent reporter gene expression by enhancing its transcriptional activity and stimulated the KLF2 promoter activity cooperatively with MEF2. Consistently, inhibition of either PI3K or AKT and depletion of AKT abrogated Ang1-induced KLF2 expression. In addition, we confirmed the dispensability of extracellular signal-regulated kinase 5 (ERK5) for Ang1-induced KLF2 expression. Furthermore, depletion of KLF2 resulted in the loss of the inhibitory effect of Ang1 on vascular endothelial growth factor (VEGF)-mediated expression of vascular cell adhesion molecule-1 in endothelial cells and VEGF-mediated monocyte adhesion to endothelial cells. Collectively, these findings indicate that Ang1/Tie2 signal stimulates transcriptional activity of MEF2 through a PI3K/AKT pathway to induce KLF2 expression, which may counteract VEGF-mediated inflammatory responses.

Angiopoietin-1 (Ang1)[2] is a ligand for endothelium-specific receptor tyrosine kinase Tie-2. Gene-targeting analyses of either *Angl* or *Tie2* in mice reveal an essential role of Ang1/Tie2 signaling in developmental vascular formation (1–3). In adult vasculature, Ang1/Tie2 signal maintains quiescence of mature blood vessels by enhancing vascular integrity and endothelial survival (4–6). However, Tie2 signaling is also involved in physiological and pathological angiogenesis, as opposed to the maintenance of vascular quiescence (4, 5, 7–9). As to this question, we and Alitalo's group (10, 11) have recently clarified that the distinct localization of Tie2 in the presence or absence of cell-cell contact determines the specificity of downstream signaling of Tie2. Ang1 induces *trans*-association of Tie2 at endothelial cell-cell contacts, whereas Tie2 is anchored to extracellular matrix by Ang1 in the absence of cell-cell contacts. *Trans*-associated Tie2 bridged by Ang1 and extracellular matrix-anchored Tie2 by Ang1 induce distinct signaling pathways preferable for vascular quiescence and angiogenesis via AKT and extracellular signal-regulated kinase (ERK) 1/2, respectively. By performing DNA microarray analysis, we also revealed that a distinct set of genes is regulated by Ang1 in the presence or absence of cell-cell contacts. Among them, Krüp-

* This work was supported by grants from the Ministry of Education, Science, Sports and Culture of Japan (to K. S., S. F., and N. M.); the Ministry of Health, Labour, and Welfare of Japan (to N. M.); and the Program for the Promotion of Fundamental Studies in Health Sciences of the National Institute of Biomedical Innovation (to S. F., T. M., T. K., and N. M.); the Naito Foundation (to S. F.); Takeda Science Foundation (to S. F.); the Sagawa Foundation for Promotion of Cancer Research (to S. F.), Mochida Memorial Foundation for Medical and Pharmaceutical Research (to S. F.), Kowa Life Science Foundation (to S. F.), Kanae Foundation for the Promotion of Medical Science (to S. F.), and Takeda Medical Research Foundation (to N. M.). The costs of publication of this article were defrayed in part by the payment of page charges. This article must therefore be hereby marked "*advertisement*" in accordance with 18 U.S.C. Section 1734 solely to indicate this fact.
♦ This article was selected as a Paper of the Week.
[S] The on-line version of this article (available at http://www.jbc.org) contains five supplemental figures.
[1] To whom correspondence should be addressed. Tel.: 81-6-6833-5012; Fax: 81-6-6835-5461; E-mail: fuku@ri.ncvc.go.jp.

[2] The abbreviations used are: Ang1, angiopoietin-1; KLF2, Krüppel-like factor 2; COMP, cartilage oligomeric matrix protein; MEF2, myocyte enhancer factor 2; ERK, extracellular signal-regulated kinase; PI3K, phosphoinositide 3-kinase; VEGF, vascular endothelial growth factor; VEGFR2, VEGF receptor 2; VCAM-1, vascular cell adhesion molecule-1; GFP, green fluorescent protein; GST, glutathione *S*-transferase; HUVEC, human umbilical vein endothelial cell; RT, reverse transcription; GAPDH, glyceraldehyde-3-phosphate dehydrogenase; HDAC, histone deacetylase; PCAF, p300/CBP-associated factor; CBP, CREB-binding protein; CREB, cAMP-response element-binding protein; BSA, bovine serum albumin; siRNA, small interfering RNA; MOPS, 4-morpholinepropanesulfonic acid; wt, wild type; mut, mutant; Luc, luciferase; CA, constitutive active.

pel-like factor 2 (KLF2) was selectively induced by Ang1 in the presence of cell-cell contacts (10).

KLF2 is a zinc finger family of transcription factor functioning in both vascular smooth muscle cells and endothelial cells and is, therefore, essential in developmental vascular formation (12–15). The *KLF2* knock-out mice exhibit impaired blood vessel formation attributable to the lack of smooth muscle cell recruitment (12). KLF2 expression in endothelium is induced by laminar shear stress and is thought to act as a molecular transducer of laminar shear stress (16–18). In the adult human vasculature, KLF2 expression is found at laminar segments of blood vessels and is decreased at branched points, which are more prone to develop atherosclerotic lesions (18), suggesting the role of KLF2 as a flow-mediated atheroprotective factor. Consistently, more than 15% of flow-regulated genes are dependent upon flow-mediated KLF2 induction (19).

It has been reported that laminar shear stress induces KLF2 expression via an ERK5-myocyte enhancer factor 2 (MEF2) signaling pathway (19, 20). The MEF2 family of transcription factors is composed of four members (MEF2A, MEF2B, MEF2C, and MEF2D) and is known as a regulator of vascular functions (21–23). Therefore, KLF2 may act downstream of MEF2 to regulate vascular functions.

KLF2 controls endothelial functions by negatively regulating inflammation and angiogenesis, thereby contributing to the maintenance of vascular quiescence (24–27). KLF2 inhibits cytokine-mediated induction of pro-inflammatory targets such as vascular cell adhesion molecule-1 (VCAM-1) and E-selectin (24, 25). In addition to anti-inflammatory action, KLF2 also down-regulates expression of vascular endothelial growth factor (VEGF) receptor 2 (VEGFR2), leading to the inhibition of VEGF-induced angiogenesis and hyperpermeability (26, 27). Similarly, Ang1 functions as an anti-inflammatory and anti-permeability factor (6, 29). Ang1 inhibits VEGF-stimulated leukocyte adhesion to endothelium by reducing expression of cell adhesion molecules such as VCAM-1 and E-selectin (30). Furthermore, Ang1 counteracts VEGF-induced hyperpermeability *in vitro* and *in vivo* (29, 31–33). Our previous data that Ang1 induced KLF2 expression (10) and the common roles by Ang1 and KLF2 for vascular quiescence prompted us to test our hypothesis that Ang1/Tie2 signal may maintain the vascular quiescence through KLF2 induction and to investigate how KLF2 is induced by Ang1/Tie2 signaling.

In this study, we found that Ang1/Tie2 signal stimulates transcriptional activity of MEF2 through a phosphoinositide 3-kinase (PI3K)/AKT pathway to induce KLF2 expression. Moreover, we revealed that Ang1-induced signaling functionally competes with VEGF-induced inflammatory responses.

EXPERIMENTAL PROCEDURES

Reagents, Antibodies, siRNAs, and Recombinant Protein—Ang1 and cartilage oligomeric matrix protein (COMP)-Ang1 were prepared as described before (34). VEGF was purchased from R&D Systems. Wortmannin and AKT inhibitor IV were obtained from Calbiochem. We generated anti-KLF2 monoclonal antibody against amino acids 2–34 of human KLF2. Anti-green fluorescent protein (GFP) antibody was prepared as described before (35). Other antibodies were purchased as follows: anti-tubulin, anti-ERK5, anti-FLAG (M2), and anti-β-actin from Sigma-Aldrich; anti-MEF2 from Santa Cruz Biotechnology; anti-phospho-AKT, anti-AKT, anti-phospho-ERK1/2, and anti-ERK1/2 from Cell Signaling Technology; horseradish peroxidase-coupled sheep anti-mouse and anti-rabbit IgG from GE Healthcare Life Sciences; and Alexa Fluor 488-labeled secondary antibody from Molecular Probes. Stealth siRNAs targeting the genes indicated below were purchased from Invitrogen: human *KLF2* (HSS145585, HSS145587), human *ERK5* (HSS140815), human *AKT1* (validated stealth RNA interference: 12935-001), human *AKT2* (validated stealth RNA interference: 12937-40), human *MEF2A* (HSS106435, HSS106436), human *MEF2C* (HSS106438, HSS106439), and human *MEF2D* (HSS106441, HSS106442). Glutathione *S*-transferase (GST) fusion protein containing transactivating domain of MEF2C (GST-MEF2C) was prepared as described before (36).

Plasmids and Adenoviruses—A luciferase reporter plasmid containing the proximal 221-bp region of KLF2 promoter (KLF2wt-Luc) was kindly provided by M. K. Jain (Case Western Reserve University). The MEF2-binding site of the KLF2wt-Luc plasmid was mutated using the QuikChange site-directed mutagenesis kit (Stratagene) using the KLF2wt-Luc vector as a template. Expression plasmids encoding MEF2C and constitutive active mutants of AKT (pCEFL-myrAKT) and PI3K-γ (pcDNA3-PI3Kγ-CAAX) and a luciferase reporter plasmid containing a single MEF2-binding site (pGL3-MEF2) have already been described (36–38). A cDNA encoding full-length MEF2C amplified by PCR using pCEFL-GST-MEF2C as a template was inserted into p3xFLAG CMV10 vector (Sigma-Aldrich) or cloned into pCMV-DBD vector (Stratagene) to construct the plasmid expressing a Gal4 DNA-binding domain (DBD)-MEF2C fusion protein (Gal4/MEF2C). Plasmids encoding Gal4/MEF2C mutant proteins (Thr-293, Thr-300, Ser-387 (phosphorylation sites by ERK5 and p38), and Thr-404 (potential phosphorylation site by AKT) were replaced with Ala, and 6 Lys residues (Lys-116, Lys-119, Lys-234, Lys-239, Lys-252, Lys-264; acetylation sites by p300) replaced with Arg were generated using the QuikChange site-directed mutagenesis kit. An expression vector encoding FLAG-tagged HDAC5 was generously obtained from C. Grozinger (Harvard University). Other vectors are purchased as follows: pRL-SV40 and pRL-TK from Promega Corp.; pEGFP-C1 from Clontech; and pFR from Stratagene. Recombinant adenovirus vectors encoding GFP and constitutively active form of AKT were kindly provided by H. Kurose (Kyushu University) and Y. Fujio (Osaka University), respectively.

Cell Culture, Transfection, siRNA-mediated Protein Knockdown, and Adenovirus Infection—Human umbilical vein endothelial cells (HUVECs) were cultured as described previously (10) and used for experiments before passage 7. HUVECs were placed on collagen-coated plates at a density of 2,000 cells/cm^2 and 40,000 cells/cm^2 and cultured overnight to obtain sparse and confluent cell cultures, respectively. U937 cells, a human monocyte-like cell line, were cultured in RPMI 1640 (Invitrogen) supplemented with 10% fetal bovine serum, 50 units/ml penicillin, and 50 μg/ml streptomycin. HUVECs were transfected using Lipofectamine 2000 reagent (Invitrogen) and Lipofectamine Plus reagent (Invitrogen) according to the manufac-

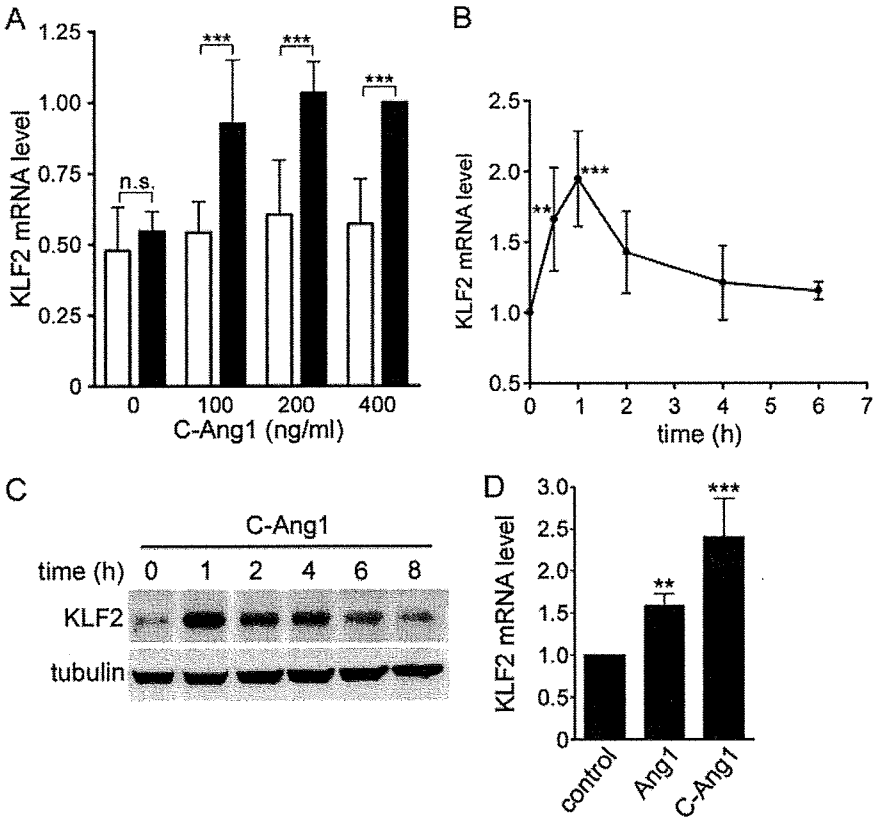

FIGURE 1. **Ang1 induces KLF2 expression in confluent HUVECs.** *A*, sparse (*open bars*) and confluent (*closed bars*) HUVECs were starved in medium 199 containing 1% BSA for 6 h and stimulated with COMP-Ang1 (*C-Ang1*) at the concentrations indicated at the *bottom* (ng/ml) for 1 h. After the stimulation, total RNA was extracted and subjected to real-time RT-PCR analysis to determine the expression level of KLF2 mRNA as described under "Experimental Procedures." Bar graphs show relative mRNA levels of *KLF2* normalized to that of *GAPDH*. KLF2 mRNA levels are expressed relative to that in confluent cells stimulated with 400 ng/ml COMP-Ang1. Data are shown as means ± S.D. of six independent experiments. *B*, confluent HUVECs starved for 6 h were stimulated with 400 ng/ml COMP-Ang1 for the periods indicated at the *bottom* (h) (COMP-Ang1 was used at the concentration of 400 ng/ml throughout the following experiments). KLF2 mRNA levels were analyzed by real-time RT-PCR as described in *A*. Values are expressed relative to that in the unstimulated cells and shown as means ± S.D. of five independent experiments. *C*, confluent HUVECs were starved in HuMedia EB2 medium containing 0.5% fetal calf serum for 12 h and stimulated with COMP-Ang1 for the periods indicated at the *top* (h). Cell lysates were subjected to Western blot analysis with anti-KLF2 (*top panel*) and anti-tubulin (*bottom panel*) antibodies. *D*, confluent HUVECs were stimulated with vehicle (*control*), 600 ng/ml Ang1 (*Ang1*), and COMP-Ang1 (*C-Ang1*) for 1 h. KLF2 mRNA levels were determined as described in *A*. Values are expressed relative to that in the control cells and shown as means ± S.D. of six independent experiments. Significant differences between two groups (*A*) or from the control (*B* and *D*) are indicated as **, $p < 0.01$ or ***, $p < 0.001$. *n.s.* indicates no significance between two groups.

turer's instructions. For siRNA-mediated gene silencing, HUVECs were transfected with siRNA duplexes using Lipofectamine RNAiMAX reagent (Invitrogen) and used for the experiments 48–72 h after transfection. HUVECs were infected with adenovirus vectors at the appropriate multiplicity of infection. Forty-eight h after infection, the cells were used for experiments.

Real-time Reverse Transcription-PCR—Sparse and confluent HUVECs placed on collagen-coated plates were starved in medium 199 containing 1% BSA for 6 h and stimulated with COMP-Ang1 as described in the figure legends. The cells were stimulated in the presence of 30 μM wortmannin or 8 μM AKT inhibitor IV. To examine the effect of COMP-Ang1 on VEGF-induced VCAM-1 expression, HUVECs starved in medium 199 containing 0.5% BSA for 5 h were prestimulated with or without COMP-Ang1 for 1 h and subsequently challenged with VEGF for 3 h. After the stimulation, total RNA was purified using TRIzol (Invitrogen). Quantitative real-time reverse transcription (RT)-PCR was carried out using QuantiFast SYBR Green RT-PCR kit (Qiagen) as described before (10). For each reaction, 100 ng of total RNA was transcribed for 10 min at 50 °C followed by a denaturing step at 95 °C for 5 min and 40 cycles of 10 s at 95 °C and 30 s at 60 °C. Fluorescence data were collected and analyzed using Mastercycler ep realplex (Eppendorf). The primers used for amplification were as follows: for human *KLF2*, 5′-CTACACCAAGAGTTCGCATCTG-3′ and 5′-CCGTGTGCTTTCGGTAGTG-3′; for human *VCAM1*, 5′-CAAATCCTTGATACTGCTCATC-3′ and 5′-TTGACTTCTTGCTCACAGC-3′; for *glyceraldehyde-3-phosphate dehydrogenase* (*GAPDH*), 5′-ATGGGGAAGGTGAAGGTCG-3′ and 5′-GGGGTCATTGATGGCAACAATA-3′. For normalization, expression of human *GAPDH* was determined in parallel as an endogenous control.

Detection of KLF2 Protein Expression—To examine the KLF2 protein expression induced by COMP-Ang1, confluent HUVECs plated on a collagen-coated dish were starved in Humedia-EB2 medium (Kurabo) containing 0.5% fetal calf serum for 12 h and stimulated with 400 ng/ml COMP-Ang1 for the periods as indicated in the figure legends. After the stimulation, the cells were washed once with ice-cold phosphate-buffered saline, harvested by scraping, and pelleted by centrifugation at 4,000 × *g* for 10 min at 4 °C. The cell pellets were then lysed at 4 °C in radioimmune precipitation buffer containing 50 mM Tris-HCl at pH 7.5, 150 mM NaCl, 1% Triton X-100, 0.5% sodium deoxycholate, 0.1% sodium dodecyl sulfate, and 1× protease inhibitor mixture. The cell lysates were subjected to SDS-PAGE and Western blot analysis as described previously (39).

Detection of ERK5, AKT, and ERK1/2 Activities—Confluent and sparse HUVECs plated on collagen-coated dish were starved in medium 199 containing 1% BSA for 6 h and stimulated with 400 ng/ml COMP-Ang1 for 15 min. The cells were then lysed at 4 °C in lysis buffer containing 25 mM HEPES at pH 7.5, 0.3 M NaCl, 1.5 mM $MgCl_2$, 0.2 mM EDTA, 0.5 mM dithiothreitol, 20 mM β-glycerophosphate, 1 mM sodium vanadate, 1% Triton X-100, and 1× protease inhibitor mixture. To meas-

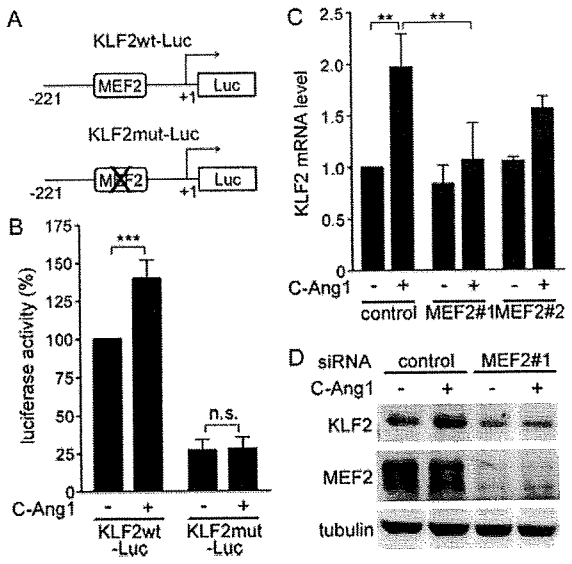

FIGURE 2. **MEF2 is responsible for Ang1-induced KLF2 expression.** *A*, structures of KLF2wt-Luc and KLF2mut-Luc reporter constructs are shown. *B*, confluent HUVECs were transfected with either KLF2wt-Luc (*left*) or KLF2mut-Luc (*right*) reporter construct together with pRL-SV40 vector. After transfection, the cells were stimulated without (−) or with (+) COMP-Ang1 (*C-Ang1*) in 1% BSA-containing medium 199 for 24 h. The medium was replaced with the freshly prepared same medium every 6 h. After the stimulation, the cells were collected, and the lysates were assayed for firefly and *Renilla* luciferase activities as described under "Experimental Procedures." The data represent firefly luciferase activity normalized by the *Renilla* luciferase activity present in each cellular lysate. Values are expressed as a percentage relative to that observed in the KLF2wt-Luc transfected cells treated with vehicle and shown as mean ± S.D. of three independent experiments. *C*, confluent HUVECs transfected with control siRNA (*control*) or with two independent MEF2 siRNA mixtures (*MEF2#1* and *MEF2#2*: each mixture contains siRNAs targeting MEF2A, MEF2C, and MEF2D) were stimulated as described in the legend for Fig. 1 (*panel D*). KLF2 mRNA levels were determined as described in the legend for Fig. 1 (*panel A*). Values are expressed relative to that in the control siRNA-transfected cells treated with vehicle and shown as means ± S.D. of three independent experiments. *D*, confluent HUVECs transfected with control siRNA or with MEF2 siRNA mixture (*MEF2#1*) were starved and stimulated with vehicle (−) or COMP-Ang1 (+) as described in the legend for Fig. 1 (*panel C*). Cell lysates were subjected to Western blot analysis with anti-KLF2 (*top panel*), anti-MEF2 (middle panel), and anti-tubulin (*bottom panel*) antibodies. In B and C, significant differences between two groups are indicated as **, $p < 0.01$, or ***, $p < 0.001$. *n.s.* indicates no significance between two groups.

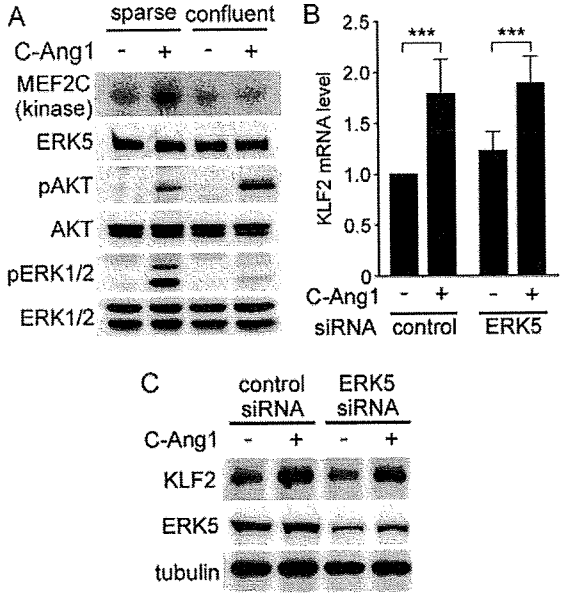

FIGURE 3. **Ang1-induced KLF2 expression does not require ERK5.** *A*, sparse (*left*) and confluent (*right*) HUVECs were starved in medium 199 containing 1% BSA for 6 h and stimulated with vehicle (−) or COMP-Ang1 (*C-Ang1*) (+) for 15 min. To measure the ERK5 activity, *in vitro* kinase assay was performed using anti-ERK5 immunoprecipitates from the corresponding cell lysates as described under "Experimental Procedures." ^{32}P-labeled substrates are shown at the *top* (*MEF2C (kinase)*). In parallel, cell lysates were subjected to Western blot analysis with anti-ERK5 (*ERK5*), anti-phosphoAKT (*pAKT*), anti-AKT (*AKT*), anti-phosphoERK1/2 (*pERK1/2*), and anti-ERK1/2 (*ERK1/2*) antibodies. *B*, confluent HUVECs transfected with control siRNA (*left*) or ERK5 siRNA (*right*) were starved and stimulated with vehicle (−) or COMP-Ang1 (+) as described in the legend for Fig. 1 (*panel D*). KLF2 mRNA levels were determined and expressed as described in the legend for Fig. 2 (*panel C*). Values are shown as means ± S.D. of five independent experiments. Significant differences between two groups are indicated as ***, $p < 0.001$. *C*, confluent HUVECs transfected with control or ERK5 siRNA were starved and stimulated as described in the legend for Fig. 1 (*panel C*). Cell lysates were subjected to Western blot analysis with anti-KLF2 (*top panel*), anti-ERK5 (*middle panel*), and anti-tubulin (*bottom panel*) antibodies.

ure the ERK5 activity, *in vitro* kinase assay was performed as described previously (40). Briefly, endogenous ERK5 was immunoprecipitated from aliquots of cell lysate with anti-ERK5 antibody at 4 °C for 3 h, and the immunocomplexes were recovered with protein G-Sepharose beads (GE Healthcare Life Sciences). Beads were washed three times with phosphate-buffered saline containing 1% Nonidet P-40 and 2 mM sodium vanadate, once with washing buffer containing 100 mM Tris at pH 7.5 and 0.5 M LiCl and once with kinase reaction buffer containing 12.5 mM MOPS at pH 7.5, 12.5 mM β-glycerophosphate, 7.5 mM $MgCl_2$, 0.5 mM EGTA, 0.5 mM sodium vanadate, and 0.5 mM sodium fluoride. Samples were then resuspended in 15 μl of kinase reaction buffer containing 3 μg of GST-MEF2C, 1 μCi of [γ-^{32}P]ATP, and 20 μM cold ATP and incubated at 37 °C for 90 min. ^{32}P-labeled substrates were separated by SDS-PAGE and detected by autoradiography. To evaluate the phosphorylation of AKT and ERK1/2, aliquots of cell lysate were subjected to Western blot analysis with anti-phospho-AKT and anti-phospho-ERK1/2 antibodies, respectively. The total contents of ERK5, AKT, and ERK1/2 in each cell lysate were also assayed in a parallel run using corresponding antibodies.

Luciferase Reporter Assay—Luciferase reporter assay was carried out as described before (36, 40). Confluent HUVECs plated on a collagen-coated 12-well plate were transfected with different expression vectors, together with reporter plasmids as described in the figure legends. The total amount of plasmid DNA was adjusted with empty vector. To examine the effect of COMP-Ang1, the cells were starved and stimulated as described in the figure legends. The cells were lysed using passive lysis buffer (Promega), and luciferase activities in cell extract were determined using a Dual-Luciferase assay system (Promega).

Detection of Subcellular Localization of FLAG-tagged HDAC5—Confluent HUVECs plated on a collagen-coated glass base dish were transfected with the plasmid encoding FLAG-tagged histone deacetylase (HDAC) 5. Twenty-four h after the transfection, the cells were starved in medium 199 containing 0.5% BSA for 6 h and subsequently stimulated with vehicle, COMP-Ang1, or VEGF for 3 h. After the stimulation, the cells were fixed and stained with anti-FLAG antibody as

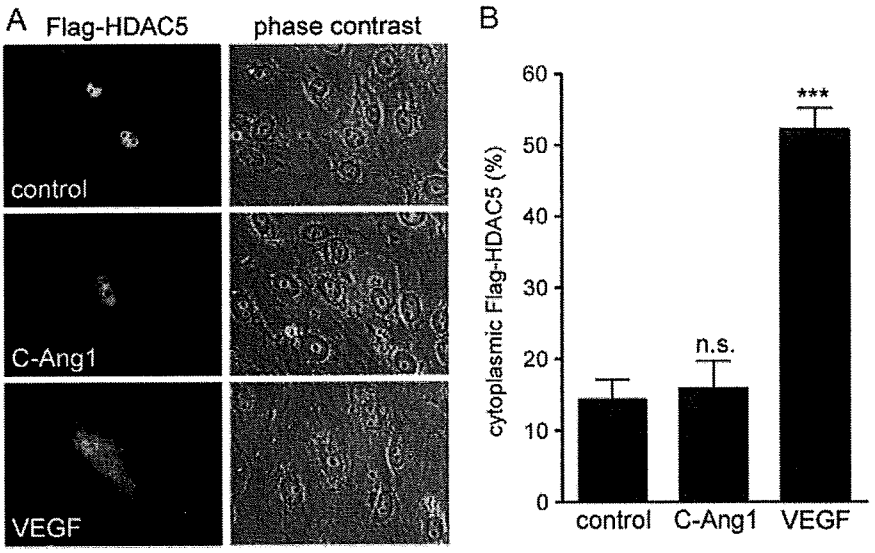

FIGURE 4. **Ang1 does not induce nuclear export of HDAC5.** *A*, confluent HUVECs plated on a collagen-coated glass base dish were transfected with the plasmid encoding FLAG-tagged HDAC5. After 24 h, the cells were starved in medium 199 containing 0.5% BSA for 6 h and stimulated with vehicle (*control: upper panel*), COMP-Ang1 (*C-Ang1: middle panel*), or 50 ng/ml VEGF (*bottom panel*) for 3 h. After the stimulation, the cells were fixed, immunostained with anti-FLAG antibody, and visualized with Alexa Fluor 488-conjugated secondary antibody. Alexa Fluor 488 and phase contrast images are shown at the *left* and *right columns*, respectively. *B*, nuclear export of HDAC5 by vehicle (*control*), COMP-Ang1 (*C-Ang1*), and VEGF observed in *A* was quantified. The number of cells expressing FLAG-tagged HDAC5 in the cytoplasm was counted and expressed as a percentage relative to the total number of cells expressing FLAG-tagged HDAC5. At least 100 cells were scored for each treatment. Values are expressed as means ± S.D. of three independent experiments. Significant difference from the control is indicated as ***, $p < 0.001$. *n.s.* indicates no significant difference from the control.

described before (10). Protein reacting with antibody was visualized with Alexa Fluor 488-conjugated secondary antibody. Alexa Fluor 488 and phase contrast images were recorded with an Olympus IX-81 inverted fluorescence microscope. The number of cells expressing FLAG-tagged HDAC5 in the cytoplasm among FLAG-tagged HADC5-expressing cells was counted. Nuclear export of HDAC5 was determined by the HDAC5 in the cytoplasm instead of the nucleus. At least 100 cells were scored for each experiment.

Monocyte Adhesion Assay—HUVECs transfected with control or KLF2 siRNA were placed on collagen-coated 24-well plates at the density of 40,000 cells/cm^2, cultured overnight, and starved in medium 199 containing 1% BSA for 2 h. The cells were prestimulated with 400 ng/ml COMP-Ang1 for 1 h and challenged with vehicle or 50 ng/ml VEGF in the presence or absence of COMP-Ang1 for 4 h. U937 cells labeled with green fluorescent dye PKH67 (Sigma-Aldrich) were added to the confluent HUVEC monolayers (8×10^5 cells/well) and incubated in RPMI 1640 containing 1% fetal bovine serum for 90 min. The cells were then washed three times with prewarmed Hank's buffered salt solution (Invitrogen) and fixed with 2% formaldehyde. Phase contrast and PKH67 fluorescent images were recorded with an Olympus IX-81 inverted fluorescence microscope. The adherent U937 cells were quantified by measuring fluorescent intensity at five randomly selected fields in each well using MetaMorph 6.1 software (Molecular Devices Corp.).

Statistical Analysis—The values are expressed as means ± S.D. Statistical significance was determined using one-way analysis of variance, two-way analysis of variance, or unpaired *t* test. *p* values < 0.05 were considered statistically significant.

RESULTS

Ang1 Induces KLF2 Expression in Confluent but Not Sparse Cultures of HUVECs—To first examine the KLF2 expression downstream of *trans*-associated Tie2 at cell-cell contacts and cell-substratum contact-anchored Tie2 in response to Ang1, HUVECs were stimulated with COMP-Ang1, a potent Ang1 variant, under either confluent or sparse culture condition. COMP-Ang1 concentration-dependently induced KLF2 mRNA expression in confluent HUVECs but not in the sparse cells (Fig. 1*A*). Consistently, KLF2 protein expression was up-regulated upon stimulation with COMP-Ang1 (Fig. 1*C*). KLF2 mRNA and protein expression by COMP-Ang1 peaked at 1 h after the stimulation and then declined to the basal level by 6 h (Fig. 1, *B* and *C*). KLF2 mRNA level was increased in response to native Ang1 as well as COMP-Ang1 (Fig. 1*D*). Taken together with the previously reported evidence that Ang1 induces *trans*-association of Tie2 in the presence of cell-cell contacts (10, 11), these results suggest that *trans*-associated Tie2 at cell-cell contacts is capable of inducing KLF2 expression.

Ang1 Induces KLF2 Expression through MEF2—Next, we sought to delineate the signaling pathway responsible for Ang1-induced KLF2 expression. It has been reported that laminar shear stress and statins activate the KLF2 promoter via a single MEF2-binding site located at −120/−111 bp upstream from the transcriptional initiation site (19, 41, 42). Thus, we investigated the role of MEF2 in Ang1-induced KLF2 expression. HUVECs were transfected with either luciferase reporter plasmid in which the reporter is driven by the proximal 221-bp region (−221 bp upstream from the initiation site) of KLF2 promoter (KLF2wt-Luc) or by its MEF2-binding site-mutated promoter (KLF2mut-Luc) (Fig. 2*A*). COMP-Ang1 significantly induced KLF2 promoter-regulated reporter activity, whereas it failed to induce reporter activation when KLF2 promoter lacked MEF2-binding site (Fig. 2*B*), suggesting the indispensable role of MEF2 in Ang1-induced KLF2 expression. To further confirm the requirement of MEF2 for Ang1-induced KLF2 expression, we employed an siRNA technique to down-regulate MEF2 family proteins including MEF2A, MEF2C, and MEF2D. Depletion of these MEF2 proteins inhibited COMP-Ang1-induced both KLF2 mRNA expression and KLF2 protein expression (Fig. 2, *C* and *D* and supplemental Fig. S1). These findings

indicate that KLF2 expression induced by Ang1 depends upon MEF2.

Ang1-induced KLF2 Expression Is Not Mediated by the Signaling Pathways Involving ERK5 and HDAC5—ERK5 stimulates transcriptional activity of MEF2 factors by phosphorylating their transactivating domains (36, 43, 44). Previous reports indicate that KLF2 expression is severely impaired in ERK5-null mouse embryo (45) and that laminar shear stress stimulates ERK5 activity to induce MEF2-dependent KLF2 expression (19). Therefore, we examined whether Ang1 stimulates ERK5 activity under either confluent or sparse conditions to investigate the involvement of ERK5 in KLF2 induction by Ang1. COMP-Ang1 preferentially activated ERK5 as well as ERK1/2 in sparse HUVECs (Fig. 3*A*). However, stimulation of confluent cells with COMP-Ang1 did not enhance ERK5 kinase activity, although AKT was potently activated under this condition (Fig. 3*A*). These results suggest that Ang1 induces KLF2 expression independently of ERK5. Consistently, depletion of ERK5 by siRNAs did not affect COMP-Ang1-induced KLF2 mRNA and protein expression (Fig. 3, *B* and *C*).

Class II HDACs, consisting of HDAC4, HDAC5, HDAC7, and HDAC9, interact with MEF2 and repress the expression of MEF2 target genes (46). Phosphorylation of class II HDACs by calcium/calmodulin-dependent protein kinase and protein kinase D results in their nuclear exclusion, leading to the enhancement of MEF2 transcriptional activity (46–48). Therefore, we examined whether Ang1 induces nuclear export of class II HDACs to enhance MEF2 activity. COMP-Ang1 did not induce nuclear export of FLAG-tagged HDAC5, although VEGF did (Fig. 4), suggesting that Ang1-induced KLF2 expression does not depend upon the inhibition of class II HDACs.

A PI3K/AKT Pathway Is Responsible for Ang1-induced KLF2 Expression—Ang1 is able to induce KLF2 expression only under confluent condition as described above (Fig. 1*A*). Under this condition, an AKT pathway is preferentially activated by Ang1 (Fig. 3*A*). These evidences prompted us to investigate whether the AKT pathway is responsible for KLF2 induction by Ang1. COMP-Ang1-induced KLF2 expression was completely blocked by wortmannin and AKT inhibitor IV, inhibitors for PI3K and AKT, respectively (Fig. 5, *A* and *B*). Furthermore, we examined the involvement of AKT in Ang1-meditaed KLF2 expression by depleting AKT using siRNAs for AKT. Depletion of AKT prevented both COMP-Ang1-induced KLF2 mRNA expression and COMP-Ang1-induced KLF2 protein expression (Fig. 5, *C* and *D*). These results indicate that a PI3K/AKT pathway is indispensable for Ang1-induced KLF2 expression.

A PI3K/AKT Pathway Stimulates Transcriptional Activity of MEF2—To clarify whether a PI3K/AKT pathway stimulates MEF2-dependent transcription, HUVECs were transfected with a plasmid expressing luciferase reporter gene under the control of a single MEF2 site (MEF2-Luc) together with the plasmid encoding constitutive active AKT (AKT-CA) or PI3K (PI3K-CA). The reporter gene activity was only slightly stimulated by AKT-CA or PI3K-CA (Fig. 6*A*). However, coexpression of MEF2C significantly enhanced AKT-CA- or PI3K-CA-induced reporter gene expression (Fig. 6*A*). To further investigate whether MEF2-dependent transcription stimulated by

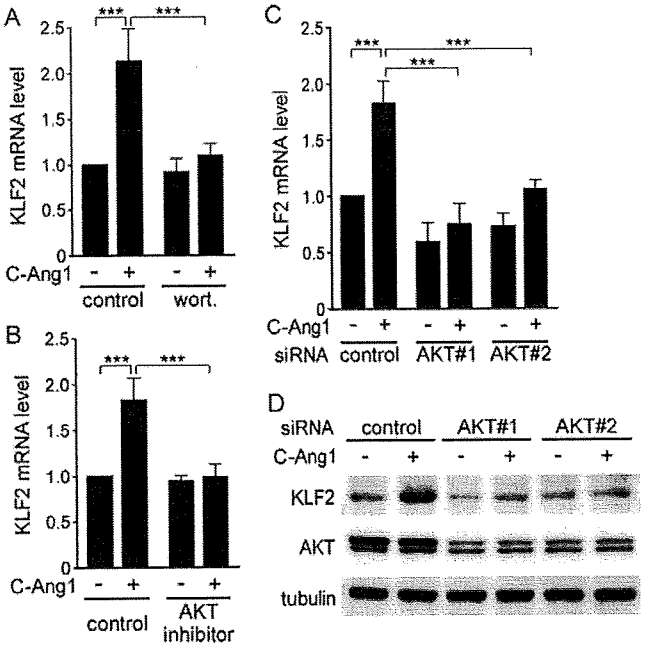

FIGURE 5. **A PI3K/AKT pathway is involved in Ang1-induced KLF2 expression.** *A*, confluent HUVECs starved for 6 h were pretreated with vehicle (*control*) or 30 nM wortmannin (*wort.*) for 30 min and subsequently stimulated with vehicle (−) or COMP-Ang1 (*C-Ang1*) (+) for 1 h. KLF2 mRNA levels were determined as described in the legend for Fig. 1 (*panel A*). Values are expressed relative to that in the wortmannin-untreated cells stimulated with vehicle and shown as means ± S.D. of five independent experiments. *B*, confluent HUVECs starved for 6 h were pretreated with vehicle (*control*) or 8 μM AKT inhibitor for 10 min and subsequently stimulated with vehicle (−) or COMP-Ang1 (+) for 1 h. KLF2 mRNA levels were determined and expressed as described in *A*. Data are shown as means ± S.D. of four independent experiments. *C*, confluent HUVECs transfected with control siRNA (*control*) or with two independent AKT siRNA mixtures (*AKT#1* and *AKT#2*: each mixture contains siRNAs targeting AKT1 and AKT2) were starved and stimulated as described in the legend for Fig. 1 (*panel D*). KLF2 mRNA levels were determined and expressed as described in the legend for Fig. 2 (*panel C*). Values are shown as means ± S.D. of four independent experiments. *D*, confluent HUVECs transfected with control siRNA or with two independent AKT siRNA mixtures (*AKT#1* and *AKT#2*) were starved and stimulated as described in the legend for Fig. 1 (*panel C*). Cell lysates were subjected to Western blot analysis with anti-KLF2 (*top panel*), anti-AKT (*middle panel*), and anti-tubulin (*bottom panel*) antibodies. In *A–C*, significant differences between two groups are indicated as ***, $p < 0.001$.

PI3K-CA and AKT-CA is ascribed to the enhanced transcriptional activity, we fused full-length MEF2C with DNA-binding domain of yeast Gal4 protein (Gal4/MEF2C) and tested the direct effect of AKT and PI3K on transcriptional activity of Gal4/MEF2C. AKT-CA and PI3K-CA potently stimulated the transcriptional activity of Gal4/MEF2C but not that of Gal4 (Fig. 6*B*). In addition, stimulation with COMP-Ang1 evoked Gal4/MEF2C-dependent reporter gene expression (Fig. 6*C*). Collectively, these findings indicate that Ang1/Tie2 signal stimulates the transcriptional activity of MEF2 through a PI3K/AKT pathway.

A PI3K/AKT/MEF2 Signaling Axis Stimulates the KLF2 Promoter—We further investigated the functional role of a PI3K/AKT/MEF2 pathway in Ang1-induced KLF2 expression. When HUVECs were transfected with the KLF2wt-Luc reporter gene along with the plasmid encoding GFP, AKT-CA, or PI3K-CA, AKT-CA and PI3K-CA induced more luciferase expression than GFP (Fig. 6*D*). The stimulatory effects of

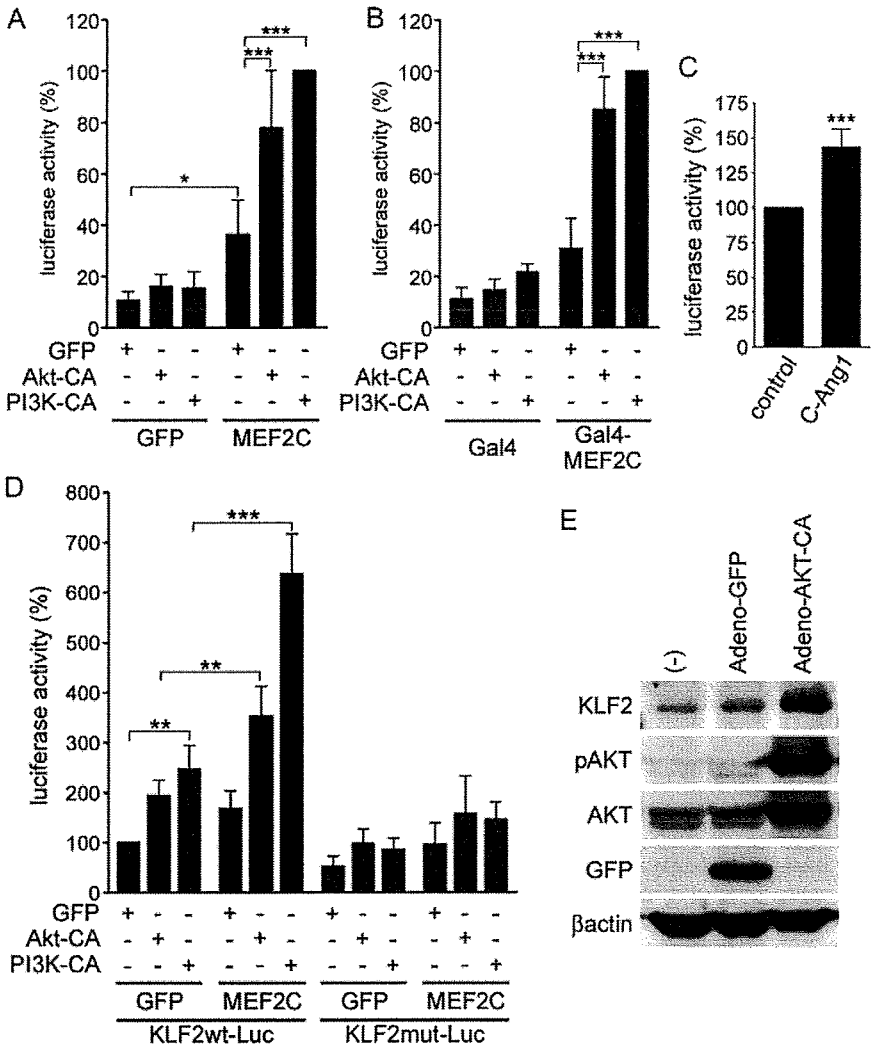

FIGURE 6. **A PI3K/AKT pathway stimulates transcriptional activity of MEF2, leading to KLF2 expression.** *A*, confluent HUVECs were cotransfected with pGL3-MEF2 and pRL-TK vectors, together with the plasmid encoding either GFP or MEF2C as indicated at the *bottom*. The expression vector for GFP, AKT-CA, or PI3K-CA was also included in the transfection mixture as shown at the *left*. The cells were lysed 24 h after the transfection. Luciferase activities were assayed and presented as described in the legend for Fig. 2 (*panel B*). Data are expressed as a percentage relative to that observed in the cells expressing both PI3K-CA and MEF2C and shown as mean ± S.D. of four independent experiments. *B*, confluent HUVECs were cotransfected with pFR and pRL-TK vectors, along with the plasmid expressing either Gal4 (*left*) or Gal4-MEF2C (*right*) as indicated at the *bottom*. The expression vector for GFP, AKT-CA, or PI3K-CA was also included in the transfection mixture as shown at the *left*. After 24 h of incubation, luciferase activities were assayed and represented as described in the legend for Fig. 2 (*panel B*). Data are expressed as a percentage relative to that observed in the cells expressing both Gal4-MEF2C and PI3K-CA and shown as mean ± S.D. of three independent experiments. *C*, confluent HUVECs transfected with the plasmid encoding Gal4-MEF2C together with pGal4-Luc and pRL-SV40 reporter plasmids were starved and stimulated as described in the legend for Fig. 2 (*panel B*). Luciferase activities were assayed and presented as described in the legend for Fig. 2 (*panel B*). Data are expressed as a percentage relative to that observed in the control cells and shown as mean ± S.D. of four independent experiments. *D*, confluent HUVECs were cotransfected with pRL-TK vector, along with either KLF2wt-Luc or KLF2mut-Luc reporter gene, and also with the expression vector for either GFP or MEF2C as indicated at the *bottom*. The plasmid encoding GFP, AKT-CA, or PI3K-CA was also included in the transfection mixture as shown at the *left*. Twenty-four h after the transfection, luciferase activities were assayed and presented as described in the legend for Fig. 2 (*panel B*). Data are expressed as a percentage relative to that in the cells transfected with KLF2wt-Luc along with the vector encoding GFP and shown as mean ± S.D. of four independent experiments. *E*, confluent HUVECs were infected without (−) or with adenoviruses encoding either GFP or AKT-CA as indicated at the *top*. Forty-eight h after infection, the cells were collected, and the lysates were subjected to Western blot analysis with anti-KLF2 (*KLF2*), anti-phosphoAKT (*pAKT*), anti-AKT (*AKT*), anti-GFP (*GFP*), and anti-β-actin (*βactin*) antibodies. Significant differences between two groups (*A*, *B*, and *D*) or from the control (*C*) are indicated as *, $p < 0.05$, **, $p < 0.01$, or ***, $p < 0.001$.

AKT-CA and PI3K-CA on the reporter gene activity were significantly augmented by coexpression of MEF2C (Fig. 6*D*). AKT-CA and PI3K-CA did not stimulate the luciferase expression driven by the mutant promoter that lacks the MEF2-binding site (the KLF2mut-Luc), even in the presence of MEF2C (Fig. 6*D*). In addition, adenovirus-mediated overexpression of AKT-CA potently induced both mRNA and protein expression of KLF2 in HUVECs (Fig. 6*E* and supplemental Fig. S2). Collectively, these results suggest that Ang1/Tie2 signal induces KLF2 expression through a PI3K/AKT/MEF2 signaling axis.

How does a PI3K/AKT signaling enhance transcriptional activity of MEF2? MEF2 activity is known to be regulated by its posttranslational modification such as phosphorylation and acetylation (49). We examined the effect of a PI3K/AKT pathway on posttranslational modification of MEF2C. We constructed the plasmids encoding Gal4/MEF2C mutants: 1) Gal4/MEF2C-ERK5/p38mut in which potential phosphorylation sites of MEF2C by p38 and ERK5 mitogen-activated protein (MAP) kinases (Thr-293, Thr-300, and Ser-387 corresponding to those in human MEF2C) were replaced by Ala (43, 50) and 2) Gal4/MEF2C-AKT mutant in which consensus phosphorylation site of MEF2C by AKT (Thr-404 corresponding that in human MEF2C) was mutated to Ala; and 3) Gal4/MEF2C-6KR in which the 6 Lys residues in MEF2C acetylated by p300 (Lys-116, Lys-119, Lys-234, Lys-239, Lys-252, and Lys-264 corresponding to those in human MEF2C) were replaced by Arg (51). Using these plasmids, MEF2-dependent transcription was directly tested in the cells expressing PI3K-CA. Expression of PI3K-CA could stimulate transcriptional activity mediated by mutant MEF2C to a similar extent to wild type MEF2C (supplemental Fig. S3). These results suggest that the posttranslational modification by ERK5, p38, AKT, and p300 is not required for PI3K/AKT pathway-stimulated MEF2 transcriptional activity.

Ang1 Inhibits VEGF-induced Inflammatory Responses through KLF2—We finally addressed the significance of Ang1/Tie2-dependent KLF2 expression in the cells. KLF2 has potent

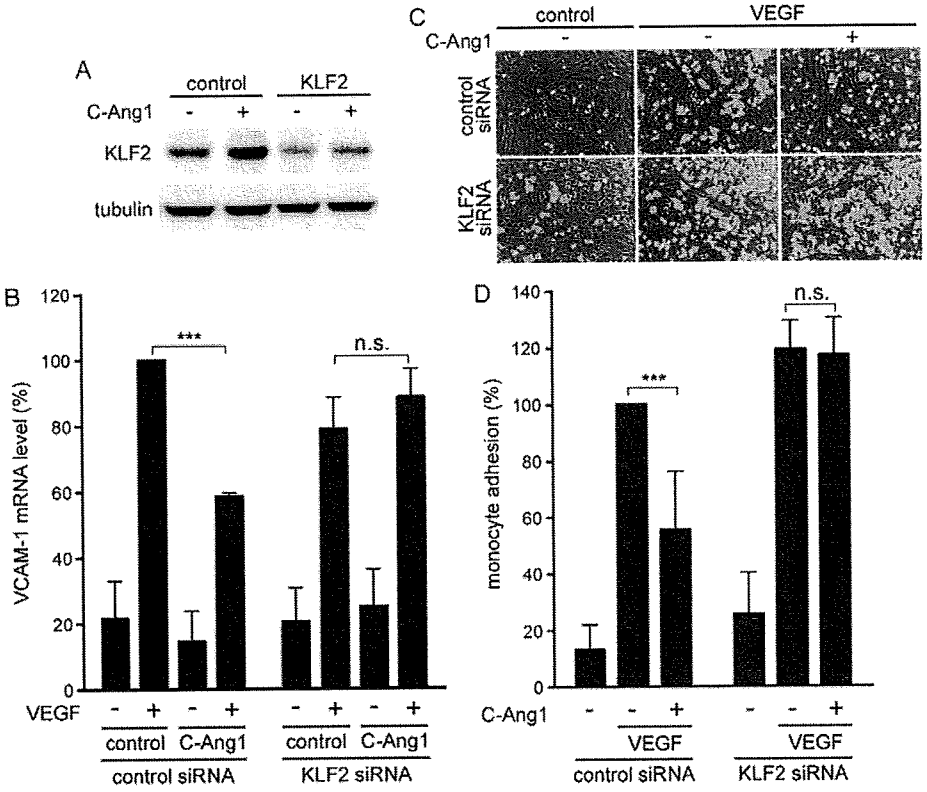

FIGURE 7. **KLF2 is responsible for the inhibitory effect of Ang1 on VEGF-induced inflammation.** *A*, confluent HUVECs transfected with control or KLF2 siRNA were starved and stimulated as described in the legend for Fig. 1 (*panel C*). Cell lysates were subjected to Western blot analysis with anti-KLF2 (*top panel*) and anti-tubulin (*bottom panel*) antibodies. *B*, confluent HUVECs transfected with control or KLF2 siRNA were starved in medium 199 containing 0.5% BSA for 6 h. The cells prestimulated with or without COMP-Ang1 (*C-Ang1*) for 1 h were challenged with vehicle (−) or 50 ng/ml VEGF (+) for 3 h. VCAM-1 mRNA levels were analyzed by real-time RT-PCR as described in the legend for Fig. 1 (*panel A*). Values are expressed as a percentage relative to that observed in the cells transfected with control siRNA and stimulated with VEGF in the absence of COMP-Ang1. Data are shown as means ± S.D. of three independent experiments. *C*, confluent HUVECs transfected with control or KLF2 siRNA were starved in medium 199 containing 1% BSA for 2 h. The cells prestimulated with (+) or without (−) COMP-Ang1 for 1 h were challenged with vehicle (*control*) or 50 ng/ml VEGF (*VEGF*) for 4 h. PKH67 fluorescent dye-labeled U937 cells were adhered to the HUVEC monolayers for 90 min. After fixation, phase contrast and PKH67 fluorescent (*green*) images were recorded with an Olympus IX-81 inverted fluorescence microscope. Shown are representative merged images. *D*, adhesion of U937 cells to HUVECs observed in *C* was quantified as described under "Experimental Procedures." Values are expressed as a percentage relative to that observed in the cells transfected with control siRNA and stimulated with VEGF in the absence of COMP-Ang1. Data are shown as means ± S.D. of four independent experiments. Significant differences between two groups are indicated as ***, $p < 0.001$. *n.s.* indicates no significance between two groups.

anti-inflammatory effects on the vascular endothelium (19, 24, 25). Ang1 also has anti-inflammatory effects and is known to counteract VEGF-induced inflammation (29, 30). Therefore, we hypothesized that Ang1 may inhibit VEGF-induced inflammation by inducing KLF2. To address this question, by depleting KLF2 using siRNA, we examined the effect of Ang1 through KLF2 on VEGF-induced VCAM-1 expression and VEGF-mediated monocyte adhesion to HUVECs. COMP-Ang1 partly inhibited VEGF-induced VCAM-1 expression and VEGF-induced adhesion of U937 cells to HUVECs (Fig. 7 and supplemental Figs. S4 and S5). However, these inhibitory effects of COMP-Ang1 were blunted by depletion of KLF2 (Fig. 7 and supplemental Figs. S4 and S5). These findings suggest that Ang1 competes with VEGF on inflammation through induction of KLF2.

DISCUSSION

Ang1/Tie2 signal is involved in both angiogenesis and vascular quiescence in adult vasculature. Recently, we and another group have shown that endothelial cell-cell contacts specify downstream signaling pathways from Tie2 (10, 11). In the presence of cell-cell contacts, Ang1 induces *trans*-association of Tie2, leading to a preferential activation of the AKT pathway. In addition, we also found that KLF2 is specifically induced by *trans*-associated Tie2. Because KLF2 is a transcription factor involved in vascular quiescence, we hypothesized that KLF2 is responsible for Ang1/Tie2 signal-mediated vascular quiescence. To address this possibility, we tried to delineate the signaling pathways involved in Ang1-induced KLF2 expression. We found that Ang1/Tie2 signal stimulates transcriptional activity of MEF2 through a PI3K/AKT pathway, which in turn induces KLF2 expression.

MEF2 plays important roles not only in muscle development but also in regulation of blood vessels (21–23). MEF2C has been implicated as a regulator of endothelial integrity and permeability (21). Interestingly, MEF2C-deficient mice exhibit a similar defect in vascular development to KLF2-null mice (52). Our present data demonstrated that MEF2 is indispensable for Ang1-induced KLF2 expression. Therefore, defect of vascular development in Ang1-deficient mice might be partly due to the lack of MEF2-dependent KLF2 induction.

Several posttranslational modifications of MEF2 in the regulation of MEF2-mediated transcription has been reported (49). Among them, ERK5 regulates MEF2 transcriptional activity by phosphorylating its transcription activation domain (36, 43, 44). Parmar *et al.* (19) have reported that flow-mediated increase in KLF2 expression occurs via an ERK5/MEF2 pathway. Because ERK5 is essential for maintaining blood vessel integrity and is known to be stimulated by Ang1 (21, 22, 53), we examined whether ERK5 acts downstream of Ang1/Tie2 to induce KLF2 expression. Unexpectedly, Ang1 only stimulated the ERK5 activity in the absence of cell-cell contacts, and under this condition, KLF2 induction by Ang1 did not occur. Furthermore, knockdown of ERK5 did not prevent Ang1-induced KLF2 expression. Therefore, ERK5 appears to be dispensable for Ang1-induced KLF2 expression.

Our data show that Ang1/Tie2 signal utilizes a PI3K/AKT pathway instead of ERK5 to induce MEF2-dependent KLF2 expression. Similarly, it has been reported that a PI3K/AKT/